**FOREIGN
BROADCAST
INFORMATION
SERVICE**

JPRS Report

DISTRIBUTION STATEMENT A

Approved for public release;
Distribution Unlimited
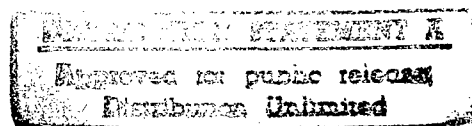
Science &
Technology

Japan

19980203 330

DTIC QUALITY INSPECTED 3

SCIENCE & TECHNOLOGY

JAPAN

CONTENTS

Nonlinear Optical Properties of Quantum Well Structure Semiconductors

[Article by Masamichi Yamanishi, Hiroshima University]

[Text] 1. Introduction

The development of highly efficient or possibly of superhigh-speed photonic switching elements (in addition to switching elements that control light with light, switching elements that control light with electrical signals) has become an important task for the construction of optical information processing systems. Such photonic switching elements would require materials with large nonlinear optical constants and possibly also with a fast response. As candidates that satisfy these conditions, the nonlinear effects of semiconductor quantum well structures or of the organic materials are being developed. The features of the nonlinear optical materials of the semiconductor quantum well structure (abbreviated as quantum well structures hereafter) are not limited simply to the large values of the nonlinear optical constant. An ordinary quantum well structure consists of a III-V compound semiconductor (for example, AlGaAs and InGaAsP), and many of the III-V compound semiconductors possess excellent electrical properties. Moreover, these electrical properties can be controlled freely to a considerable degree. In other words, in quantum well structures it is possible to introduce electrical means to the intrinsic optical nonlinearity to further strengthen the optical nonlinearity or let the electronic elements and the photonic switches coexist. In addition, a significant advantage is the fact that the operating wavelengths for the nonlinear optical operation are compatible with the emission wavelengths of the semiconductor lasers that are currently the most practical light sources. From this viewpoint, this article will present only the optical nonlinear effects of the quantum well structures that are related in some sense to the electrical properties. More specifically, a certain kind of electrooptic effect called quantum confined Stark effect (QCSE), various kinds of optical nonlinear elements with self-positive-feedback mechanism obtained by combining electrical means with the QCSE, and superhigh-speed optical nonlinear effect (generation of hypershort electrical pulses, in particular) due to virtually excited carriers in quantum well structures under an electric field, will be described briefly.

2. Quantum Confined Stark Effect[1]

(a)

(b)

Figure 1. Energy Band Diagrams for
Quantum Well Structure
Quantum levels and the wave
functions are depicted in the
(a) absence of an electric
field and (b) presence of
an electric field.
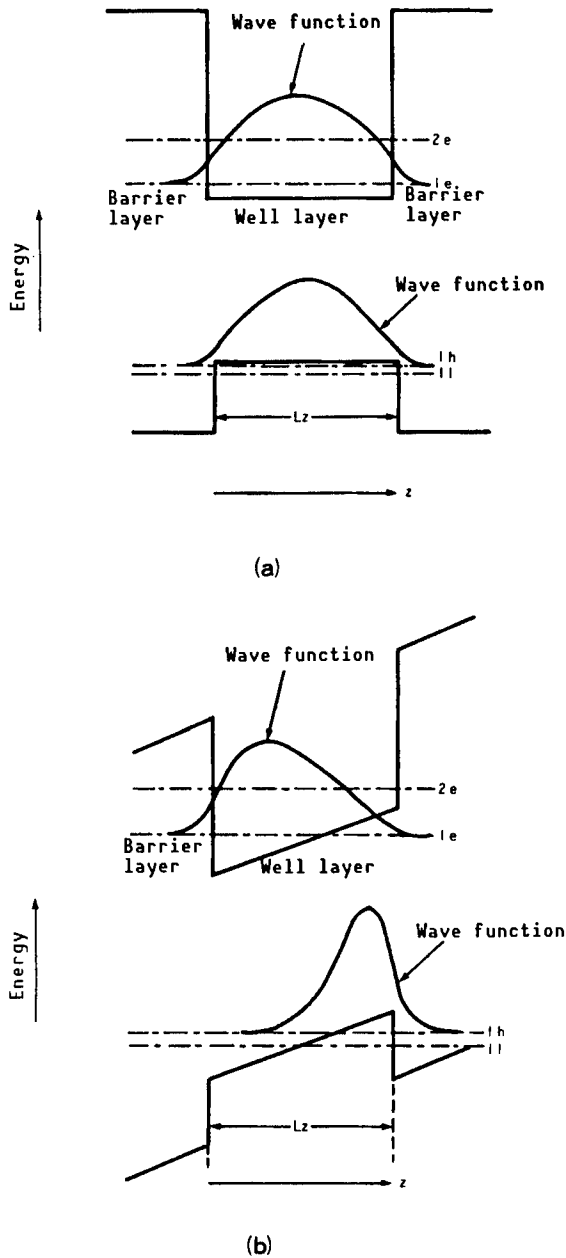
In a quantum well structure not under an electric field, the absolute values of the wave function of the conduction band and the valence electron band are symmetrical with respect to the center of the well, as shown in Figure 1(a). Next, when an electric field is perpendicular to the well plane of the quantum well structure, the form of the wave functions becomes asymmetrical, as indicated in Figure 1(b). At the same time, a quantum level of the conduction band (for example, level 1e in the figure) is lowered relatively, whereas a quantum level of the valence electron band (for example, level 1h in the figure) is raised relatively. Such deformations of the wave functions and changes of the quantum levels due to applied electric field bring about changes in the oscillator strength and the transition energy (red shift) for light. Further, in a quantum well, the excitons remain stable even under a fairly strong perpendicular electric field ($\sim 10^5$V/cm). They will not be decomposed by the electric field of this order since they are placed between sufficiently high barriers. In fact, even under a strong electric field of the order that generates a peak shift of several times the exciton coupling energy of about 10 meV in the absence of an electric field, absorption peaks of the excitons continue as shown in Figure 2.[2]

Such stable behavior of the excitons within a quantum well in the presence of a perpendicular electric field is called quantum confined Stark effect.
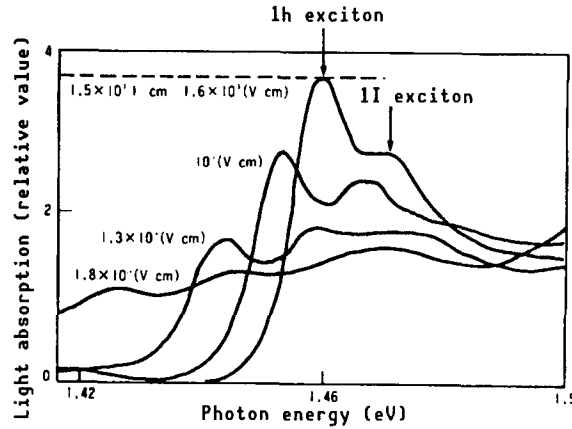
Figure 2. Changes Due to Electric Field of Absorption Spectra of
AlGaAs/GaAs Quantum Well Structure at Room Temperature[2]

A small light-intensity modulator with high speed (switching time of 100 psec, which is determined by the C-R time constant) is achieved by utilizing the large change in the light absorption due to the perpendicular electric field described above (in the case of Figure 2, for an incident photon energy of 1.44 eV, an applied electric field of 1.3×10^5 V/cm causes a change in the absorption coefficient of about 5,000 cm^{-1}).[1] Further, the light absorption spectrum and the refractive index spectrum are mutually related by the Kramers-Kronig relation so that the refractive index of a quantum well structure varies markedly with the electric field (change of the refractive index in the neighborhood of the exciton gap wavelength being 4 percent).[3] Phenomenologically, for a typical quantum well structure (AlGaAs/GaAs and a well thickness Lz of about 100 Å) and an applied electric field of the range of up to 5×10^4 V/cm, and when the incident photon energy is several tens of millielectron volts less than the exciton gap energy in the absence of an electric field, the change of index of refraction Δn is proportional to the square of the electric field E_0 and to the inverse square of the detuned energy Δ (that is, $\Delta n \propto E_0^2/\Delta^2$).[4] Namely, the change in the index of refraction due to the QCSE effect can phenomenologically be regarded as a kind of Kerr effect, and hence can be represented by $X^{(3)}$ (ω: $-\omega$, 0, 0). The value of $X^{(3)}$ in a AlGaAs/GaAs quantum well of Lz~100 Å, for example, is $X^{(3)}$ (ω: $-\omega$, 0, 0) = 1.8×10^{-8}(esu) for Δ = 42 meV.[4,15] Further, in the case of observing the index of refraction change for minute changes of the electric field for a fixed bias electric field E_0, the phenomenon may be regarded as a kind of Pockel's effect, and hence can be represented by $X^{(2)}$ (ω: $-\omega$, 0) $\approx$ $2X^{(3)}$ (ω: $-\omega$, 0, 0) x E_0. For example, when applying a bias electric field of $E_0 = 8 \times 10^4$ V/cm to an AlGaAs/ GaAs quantum well structure with Lz = 120 Å, the result is $X^{(2)}$ (ω: $-\omega$, 0) = 5×10^{-5} (esu) for a detuned energy Δ' = 15 meV from the exciton gap of the bias state. Various high-speed optical switch elements that utilize such a large Kerr effect (or a Pockel's effect) are being examined.[1,16] Moreover, in the case of perpendicular electric field arrangement, even when the quantum well structure is a multiquantum well structure laminated in the direction of the thickness, it only needs to induce an electric field by applying an electric field to a layer structure with the total thickness of about 1 μm at

the most. Accordingly, in the case of a p-n junction structure, a strong electric field of about 1×10^5V/cm can easily be generated with an applied voltage of less than 10 V. This point is an important feature for applying QCSE from a perpendicular electric field to a quantum well structure with excellent electrical properties and size control.

3. Nonlinear Elements by Self-Positive Feedback

Using a strong electrooptic effect (QCSE) as described in the previous section raises the possibility of an optical bistable element due to the positive feedback mechanism by electrically enhancing the optical nonlinear effect, thus eliminating the need for an optical resonator. The first attempt to fabricate an optical nonlinear element of this kind was undertaken by Miller, et al.,[7] at Bell Labs. As shown in Figure 3(a), these workers applied a reverse bias voltage via a large resistance R to a p-i-n diode in which a multiple quantum well structure is buried in its i layer. By irradiating the diode with light having a wavelength that coincides with the peak wavelength of the exciton in a weak electric field, they discovered in the transmitted light versus incident light characteristic an optical bistability as shown in Figure 4.
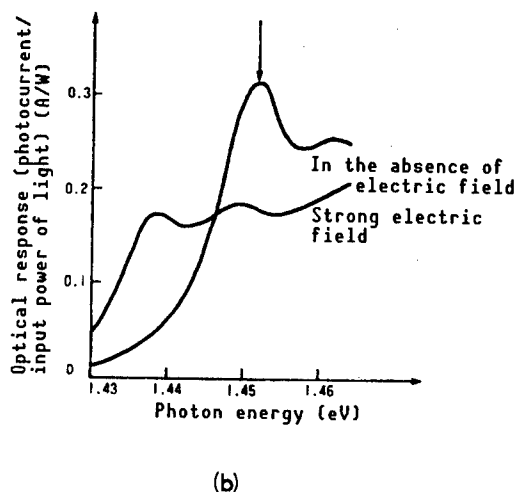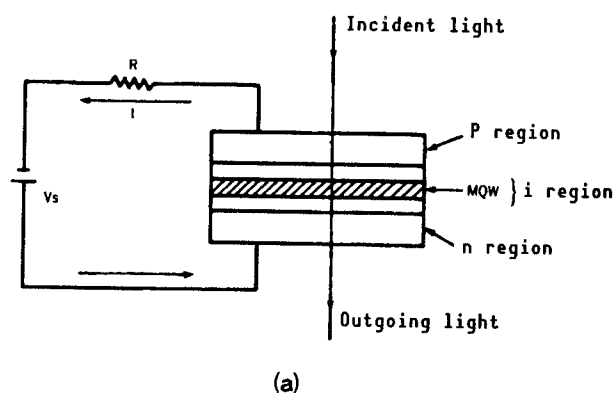

(a)

Figure 3. Explanatory Diagram for
(a) Element Constitution and
(b) Principle of Operation of SEED[7]
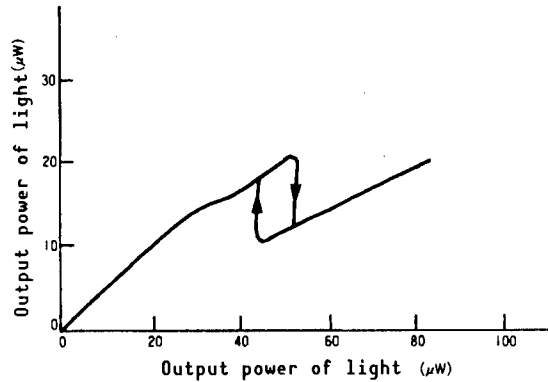The arrow in (b) indicates the photon energy of the incident light.

(b)

4

Figure 4. Experimental Data Showing Optical
Bistability of SEED[7]

Its positive feedback mechanism is as described below. Assume that the wave-
length of the incident light coincides with the excitation peak wavelength in
a weak electric field, when a sufficiently large reverse bias voltage is
applied to the diode. When the power of the incident light is increased in
this state, the photocurrent is increased, and as a result, the reverse
voltage applied to the diode is reduced because of the drop in the voltage
applied to the load resistor R. At this time, as shown in Figure 3(b), the
photocurrent increases in spite of the decrease of the bias voltage to the
diode (this being a kind of negative resistance characteristic). The increase
in the photocurrent enhances the voltage drop in the resistor R, causing the
reverse voltage to be reduced further. By repeating the positive feedback, the
diode is switched in one step from high voltage and low absorption to low
voltage and high absorption. In this element, the self-positive feedback
mechanism due to the combination of the electrooptic effect in the quantum
well structure within the diode and the load resistor is playing a key factor
in the operation of the element. In this sense, this element is called a self-
electrooptic effect device (SEED).[7] In a SEED, the input light energy necessary
for the optical bistability is very small (3~10 fJ/μm^2),[7] but the time required
for switching becomes greater than 100 ns. Such a long switching time is
required because the switching time element is determined by the product of
the load resistance R and the electrostatic capacitance C of the diode, and
because a considerably large resistance (R≥100 kΩ) is required for the
bistable characteristic. Although the slow switching speed may be tolerable in
some applications, load resistors larger than 100 kΩ are most undesirable for
integrating a large number of these elements on a two-dimensional surface.
Several attempts have been made to eliminate this disadvantage of SEEDs.

The author and his coworkers have attempted to obtain a positive feedback by
combining the electrooptic effect of a quantum well structure and the charge
polarization of optically excited carriers.[8] For example, when a whole multiple
quantum well structure is placed between barrier layers with sufficiently
large band gap, photoexcited electrons and holes will not recombine within the
multiple quantum well structure but accumulate at both ends, forming a charge
polarization (Figure 5).

5

Multiple quantum well
structure with 20 cycles
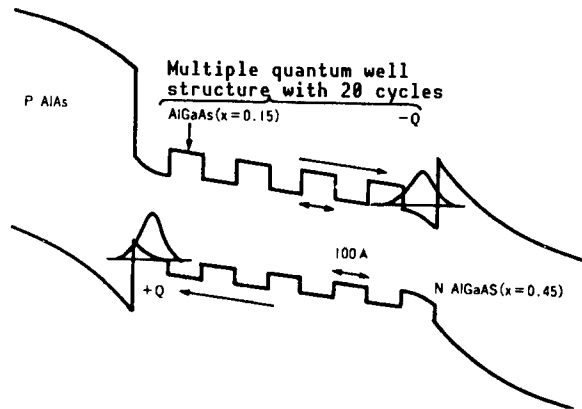AlGaAs(x = 0.15)   -Q

100 A

N AlGaAs (x = 0.45)

+Q

Figure 5. Example of the CSF Effect in Energy Band Diagram of
AlGaAs/GaAs Multiple Quantum Well Structure Biased
by an Electric Field

The charge polarization generates a counter electric field with reverse polarity, and the electric field within the multiple quantum well structure is diminished. If the wavelength of the incident light coincides with the wavelength of the exciton for low electric field, the light absorption coefficient is increased because of the decrease of the electric field. Such an increase in light absorption increases the number of accumulated carriers at both ends of the multiple quantum well structure and weakens the electric field further. In this way, the electric field of the multiple quantum well is reduced to a low value in one step. In this case, different from the case of a SEED, a diode with a built-in multiple quantum well structure must be connected directly to a bias power supply without an intermediate series of resistors. Such a positive feedback mechanism, due to charge polarization, is called charge-induced self-feedback (CSF).[8] Figure 6 shows experimental data on the CSF effect.[9] For a low input power density of about 1 W/cm^2, light absorption increases very rapidly, and it was confirmed that a positive feedback actually takes place without requiring an external resistor as mentioned above. In addition, the optical bistability phenomenon due to the CSF effect was observed at room temperature very recently (Katsuhiro Obata, et al., scheduled to be presented at the spring meeting of the Japan Society of Applied Physics, 1990).

Light input power (mW)
0   2   4   6   8

Room temperature
Bias
    voltage: -8.0V

858nm

Output power (arbitrary unit)

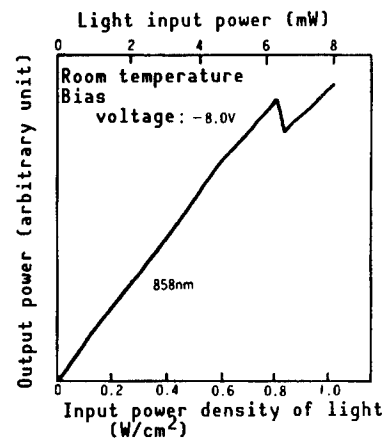0   0.2   0.4   0.6   0.8   1.0
Input power density of light
(W/cm^2)

Figure 6. Experimental Data Showing the CSF
Effect[9]
(a) Photocurrent
(b) Transmitted output vs.
incident light power

Here, let us examine the positive feedback mechanism due to charge polarization in a more quantitative way. Between the surface density N_s of electrons and holes accumulated at both ends of the multiple quantum well structure and the counter electric field E_s generated due to charge polarization of the accumulated carriers, the following relation holds:

$$E_s = eN_s/\epsilon_0\epsilon_s,$$

where e, ϵ_0, and ϵ_s are the electron charge, dielectric constant of the vacuum, and relative dielectric constant of the medium. Further, the optical energy per unit area expended within the multiple quantum well structure for generating the electron–hole pairs of the surface density N_s is $(\hbar\omega_p) \cdot N_s$ where $\hbar\omega_p$ is the photon energy. The light power (I_{pin}) needed to keep the electron-hole pairs stationary is given by

$$I_{pin} = (\hbar\omega_p)N_s/\tau,$$

where τ is the outflow time from the multiple quantum well structure to the barrier layers on the outside. When an element has the structure shown in Figure 5, the relations given above and the experimental data in Figure 6 show the response time to be $\tau = 460$ nsec and the switching energy $I_{pin} \cdot \tau$ about 1 fJ/μm^2.[9] A faster response can be obtained by reducing τ (specifically, by reducing the height of the barrier layers shown on the outside in Figure 5). It should be noted, however, that even then the switching energy $I_{pin} \cdot \tau = (\hbar\omega_p) \cdot N_s$ would remain. The switching energy of about 1 fJ/μm^2 obtained for this case is comparable to the switching energy 3~10 fJ/μm^2 reported for SEEDs.[7] This is no coincidence.[10] In a SEED, different from a CSF device, the multiple quantum well structure is not sandwiched by barrier wall layers with a wide band gap. Because of this, the electrons and holes optically excited in the quantum well structure can easily escape the multiple quantum well structure and reach the terminal electrode of the diode. Since, however, a large resistance is connected in series to the diode, the $C \cdot R$ time constant determines the time it takes the electrons and holes to escape to the outside of the diode. Thus, in a SEED, the electrons and holes induce a charge at the electrode part of the pin diode, and as a result, the internal electric field of the diode is diminished. Considered in this way, one may say that the positive feedback mechanisms of a CSF device and a SEED are equivalent under a simple interchange of the product $C \cdot R$ and the outflow time τ.

Another method for realizing the positive feedback was proposed by Sakaki, et al.[11] Differing from the case of a SEED, bistable operation was achieved by serially connecting a negative resistance element such as a tunneling diode and a diode with built-in multiple quantum well structure. Accordingly, there are no special restrictions on the wavelength of incident light on the multiple quantum well diode. Further, since it is possible to freely design the negative resistance element separately from the multiple quantum well structure, it is possible to expect a high-speed operation ($C \cdot R = 10$ psec) at a high extinction ratio (19:1), and a low switching energy of 1 fJ/μm^2 can be estimated.[11] This device is called a bistable optical negative resistance device (BOND). The bistable operation of the element is confirmed at 80 K[12] and at room temperature.[13] However, designing the negative resistance element

7

requires special consideration because a considerably higher range of voltage is needed to generate the negative resistance. In all of the above-mentioned cases of SEED, CSF, and BOND, the device can be operated with a low switching energy ($\sim$ fJ/cm^2) comparable to various kinds of transistors. This is because in both transistors and optical switches the potential change due to charge polarization eventually plays the fundamental role.

4. Superhigh-Speed Optical Nonlinearity Due to Virtual Charge Polarization

The switching time of the optical switches described above is limited by the C·R time constant or the life of the carriers as in a CSF device. The author[14] and Chemla, et al.,[15] of Bell Labs have proposed a method for switching an electric field in a quantum well structure in an ultrashort time range of several hundred femtoseconds, which eliminates at a stroke the restrictions of the C·R time constant and the carrier life. In a quantum well structure under the influence of a dc electric field E_0 as shown in Figure 7, when the photon energy $\hbar\omega_p$ of incident light is sufficiently smaller than the exciton gap energy, a charge polarization is generated by virtual excitation within the quantum well structure, as shown by the broken line in the figure. Since the photoexcitation process is virtual, it can respond fast enough (within about 100 fsec) for both the on and off of an incident light pulse. A charge polarization due to virtual carriers thus produced generates a counter electric field and cancels the originally applied electric field to some extent. Since this process is also generated by the charge polarization within the quantum well, it is extremely fast (it will not be limited by the C·R time constant). This optical nonlinearity due to virtual charge polarization is called virtual charge-induced optical nonlinearity (VCON).[14]
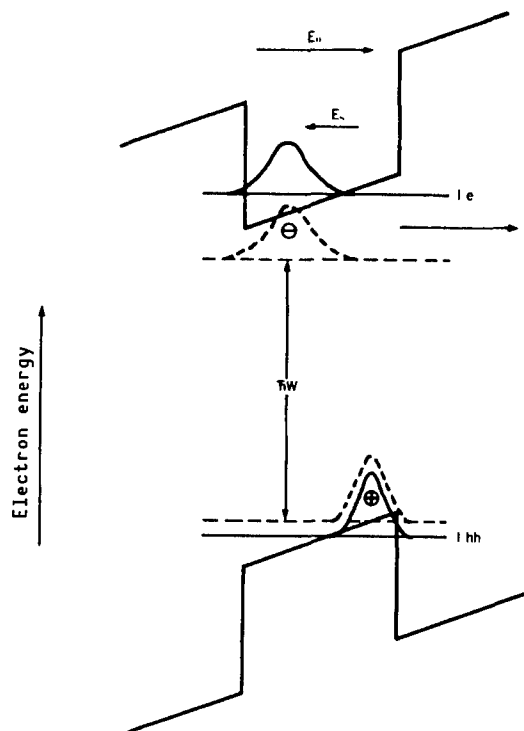

Figure 7. Explanation of VCON Process by Reference to Energy Band Diagrams for a Quantum Well Structure Biased by an Electric Field[14]

8

A process that produces an internal electric field modulation E_s is a kind of light rectification (or inverse linear electrooptic effect). The virtual polarization $P = \epsilon_0 \epsilon_s E_s$ can be represented with a second-order or a fourth-order nonlinear coefficient by the following equation:

$$P = \epsilon_0 \epsilon_s E_s = \epsilon_0 X^{(2)} \ (0: \ \omega, \ -\omega) \ E_p^2$$
$$\approx \epsilon_0 X^{(3)} \ (0: \ 0, \ \omega, \ -\omega) \ E_0 \cdot E_p^2,$$

where E_p is the electric field of the incident light. Since in general the cyclic permutations of the arguments of the coefficients $X^{(2)}$ and $X^{(3)}$ leave the values of $X^{(2)}$ and $X^{(3)}$ invariant,[17] the following relations hold:

$$X^{(2)} \ (0: \ \omega, \ -\omega) = X^{(2)} \ (\omega: \ -\omega, \ 0)$$

$$(\tfrac{1}{2}) \ X^{(3)} \ (0: \ 0, \ \omega, \ -\omega) = X^{(3)} \ (\omega: \ -\omega, \ 0, \ 0)$$

that is, $X^{(2)}$ or $X^{(3)}$ that represents the virtual change polarization of the quantum well structure is equal to $X^{(2)}$ or $X^{(3)}$ that represents QCSE described in section 2. Accordingly, the value of $X^{(2)} \ (0: \ \omega, \ -\omega)$ or $X^{(3)} \ (0: \ 0, \ \omega, \ -\omega)$ is far smaller than that of a bulk crystal. The most characteristic point will be the generation of ultrashort electric pulses based on an ultrafast internal electric field modulation. If it becomes possible to generate electric signals of subpico seconds, which has been difficult with current electronic technology, a major impact on the future of optoelectronics in the femtosecond range can be expected. An experimental generation of such an ultrashort electric pulse is being attempted[18]; however, since it is still in the initial stages, the process has yet to be evaluated.

5. Conclusion

The characteristic common to all of the examples given in this paper on the optical nonlinear effects of the quantum well structure is not only limited to the interactions of the system of light and the electron, but is attempting to enhance the nonlinear effect by interposing an electrical effect in the system. Rapid progress is being made not only in the actual excitation of carriers but also in the superhigh-speed processes induced by virtual excitation. This progress is desirable for enhancing the integrated circuit functions by combining light and electronic circuits. As to the optical nonlinearity due to the real and virtual excitations independent of electrical signals, the reader is referred to a recent exposition.[19] Moreover, remarkable advances have been made recently in the optical nonlinearity of pseudo-zero dimensional systems (quantum box, quantum dot, microcrystal, and the like) with an increased dimension of quantum confinement. Regarding this point the reader is referred to another recent exposition.[20]

References

1. For example, as an exposition of QCSE, see L. Esaki, supervisory editor, and edited by M. Sakaki, "Superlattice Heterostructural Devices," Chapter 19, (by M. Yamanishi), published by Association of Industrial Investigations.

2. Weiner, J.S., Miller, D.A.B., Chemla, D.S., Damne, T.C., Burrus, C.A., and Wood, T.H., APPL. PHYS. LETTERS, Vol 47, 1985, p 1148.

3. Nagai, H., Kan, Y., Yamanishi, M., and Suemune, I., JPN. J. APPL. PHYS., Vol 25, 1986, p L640.

4. Weiner, J.S., Miller, D.A.B., Chemla, D.S., APPL. PHYS. LETTERS, Vol 50, 1987, p 842.

5. Yamanishi, M., to be published in Proc. OSA Topical Meeting on Picosecond Electronics and Optoelectronics, March, 1989, Salt Lake City.

6. Zucker, J.E., Jones, K.L., Young, M.G., Miller, B.I., and Koren, U., Proc. OSA Topical Meeting on Photonic Switching, March 1989, p 22.

7. Miller, D.A.B., Chemla, D.S., Damen, T.C., Wood, T.H., Burrus, C.A., Gossard, A.C., and Wiegman, W., IEEE J. QUANTUM ELECTRON., Vol QE-21, 1985, p 1462.

8. Yamanishi, M., Lee, Y., and Suemune, I., OPTOELECTRONICS-DEVICES AND TECHNOLOGIES, Vol 2, 1987, p 45.

9. Kan, Y., Obata, K., Yamanishi, M., Funahashi, Y., Sakata, Y., Yamaoka, Y., and Suemune, I., JPN. J. APPL. PHYS., Vol 28, 1989, p L1585.

10. Schmitt-Rink, S., "Linear and Nonlinear Optical Properties of Semiconductor Quantum Wells," ADVANCES IN PHYSICS, Vol 38 No 2, 1989, p 89.

11. Sakaki, H., Kurata, H., and Yamanishi, M., ELECTRON. LETTERS, Vol 24, 1988, p 1.

12. Kurata, H., Tsuchiya, M., Sakaki, H., presented at Int. Conf. Modulated Semiconductor Structures, Ann Arbor, Michigan, July 1989, to be published in Proc. of MSS.

13. Amano, C., Matsuo, S., and Hasumi, Y., Fall 1989 Meeting of the Japan Society of Applied Physics, No 271-ZH-7/III.

14. Yamanishi, M., PHYS. REV. LETTERS, Vol 59, 1987, p 1014.

15. Chemla, D.S., Miller, D.A.B., and Schmitt-Rink, S., Ibid., p 1018.

16. VCON Process in detail, please refer to Masamichi Yamanishi, APPLIED PHYSICS, Vol 58, 1989, p 1696.

17. For example, N. Bloembergen, NONLINEAR OPTICS, W.A. Benjamin Inc., 1965, pp 9–11.

18. Knox, W.H., Henry, J.E., Tell, B., Li, K.D., Miller, D.A.B., and Chemla, D.S., OSA Topical Meeting on Picosecond Electronics and Optoelectronics, March 1989, oral presentations.

19. Shimizu, A. and Fujii, K., KOTAIBUTSURI, Vol 24, 1989, p 846.

20. Hiroshima, M. and Hanamura, E., Ibid., p 839.

Nonlinear Optical Effects of Optical Fibers

[Article by Masataka Nakazawa, NTT Transmission System Laboratory: "Nonlinear Optical Effects of Optical Fibers and Applications for Optical Communications"]

[Text] 1. Introduction

Numerous basic research projects are exploring a wide range of practical applications for future communications systems using optical fibers as well as ultrahigh capacity, long-range, and repeaterless optical transmission. In many countries these projects concern nonlinear optical effects of a silica optical fiber, focusing on its special characteristics of low loss (about 0.2 dB/km for the wavelength band of 1.5 μm), high light intensity that can be confined in a narrow cross sectional area, and the property of permitting a large interaction length.[1] This article will survey these nonlinear optical effects and show how they are being applied to optical communications. In particular the article will address the optical soliton,[2] which has become a recent topic of interest, focusing on how to realize it within the optical fiber as well as its applications.

2. Nonlinear Optical Effects in Optical Fiber

For several reasons, nonlinear optical effects become conspicuous in the optical fiber:

(1) A high light intensity becomes available because of the confinement of light in a narrow cross sectional area,

(2) Light has waveguide modes whose interaction length can extend up to several kilometers,

(3) In a single-mode silica fiber, the loss is low at about 0.2 dB/km, etc.[1]

To measure nonlinear optical effects in ordinary bulk materials, an optical beam is converged using an optical lens, but in this case, if the beam is condensed too drastically, the beam will diverge rapidly after converging.

Because of this, the product of the power density and the interaction length, which are important parameters for increasing the nonlinear optical effect, becomes constant, so that eventually there is no way to increase the nonlinear optical effect but by increasing the incident power. However, in the case of a waveguide such as an optical fiber, the spot size of the lateral mode and the fiber length, namely the interaction length, can be controlled independently so that it is easy to generate the nonlinear optical effect. Further, by appropriately controlling the structural distribution or the material distribution, it becomes possible to phase match an excited light and a signal light so that the nonlinear phenomenon which has been difficult to generate in a bulk material can be achieved.

Table 1. Comparison of Characteristics of Nonlinear Interactions for Optical Fibers and Bulk Materials

Item	Waveguide including optical fibers	Bulk materials
Excitation power density	High ($10^7 \sim 10^8$ times that of bulk materials)	Low
Phase matchability	Distribution of waveguides usable (phase matching is possible even for isotropic medium)	Uses birefringence
Interaction length (L)	Long	Short
Loss	Relatively large except for silica optical fibers	Small
Wavelength region	Restricted by the cutoff wavelength	Wide
Converted output	Low output because of small mode volume	High output
Nonlinear material	Limited to those that can be made into waveguides	Many different kinds
Compact packaging	Easy	Difficult
Manufacture	Requires techniques for putting it to waveguides	Easy
Integration with multifunctional device	Possible	Difficult

For these reasons, the peak power of several milliwatts (MW) that was needed to generate a nonlinear effect in a bulk material can be reduced to a low excitation input of less than 1 W in an optical fiber. Since a peak power of this order is fully realizable in the near future considering the recent advances of the semiconductor laser technology, the application of nonlinear optical effects to functional devices has a fairly high feasibility. Table 1 compares the characteristics of the nonlinear interactions for optical fibers (including waveguides) and bulk materials. As shown in the table, the bulk materials are advantageous for obtaining large converted output, but the optical fibers are desirable for realizing high conversion efficiency with low

excitation input. Nonlinear optical phenomena in the representative optical fibers and their applications reported so far are shown in Table 2. The stimulated Raman scattering[3] and the stimulated Brillouin scattering[4] that are generated by the imaginary part of the third-order term $X^{(3)}$ of the nonlinear polarization can fully be realized with light intensity of about 1 W for single-mode fibers. Using the light amplification characteristics of these phenomena, not only have lasers of continuous oscillation been achieved, but short optical pulses have been generated by the mode-locking technique.

Table 2. Nonlinear Optical Phenomena in Optical Fibers and Their Applications

Phenomenon	Applications
Stimulated Raman scattering / Stimulated Brillouin scattering	Wavelength conversion, Light-light amplification, Wavelength variable lasers, Mode-locking lasers, Phase conjugation
Four-photon mixing	Parametric light amplification, Pressure and temperature sensors
Optical Kerr effect	Waveform shaping, Optical shutter, Light intensity modulation
Self-phase modulation effect	Optical pulse compression, Optical soliton, Modulation instability
Photo-induced refractive index change	Phase lattice, DFB lasers, Narrow band optical filters
Second harmonic generation / Sum-frequency light generation	Wavelength conversion, Use for dye lasers, Light source

The nonlinear optical effect of the real part of $X^{(3)}$ is a parametric light amplification (induced four-photon mixing) that requires a phase matching.[5] In addition, nonlinear refractive index phenomena that depend on light intensity of the effect include the self-phase modulation effect, optical pulse compression, propagation of optical soliton, and the like. The nonlinear effects due to $X^{(2)}$, second harmonic generation, and sum-frequency light generation, are realized in $LiNbO_3$ light waveguides with diffused Ti or in single crystal fibers. Further, the second harmonic generation and the sum-frequency wave generation are also possible in single-mode silica fibers with their efficiencies reaching about 1 percent.[6] The next sections will describe individual optical effects.

14

3. Stimulated Raman Scattering

Stimulated Raman scattering (SRS) occurs when a monochromatic excitation light irradiates a material, and mixed in the scattered light is a coherent Stokes radiation whose wavelength is shifted from that of the matter in accordance with the frequency of the incident light as a result of its interaction with the optical phonons of the material. In general, Raman scattered light is polarized strongly in the same direction as the polarization direction of the incident light, and the polarized component perpendicular to the polarization direction of the incident light is extremely weak. Further, in noncrystalline materials such as optical fibers, the spectral width is wider and the peak intensity is lower than those of crystalline materials. In Figure 1 are shown Raman spectra of various oxide glasses of GeO_2, P_2O_5, B_2O_3, $Na_2 \cdot 2SiO_2$, and SiO_2. The result in the figure shows the gain coefficient of each glass normalized with respect to the Raman gain coefficient of SiO_2. The Raman gain coefficient of SiO_2 is 1×10^{-11}cm/W in the case of a Stokes shift of about 440 cm^{-1} due to excitation with light of wavelength 1 μm. Since a GeO_2 fiber has a gain about nine times that of SiO_2, it is being studied intensively as a nonlinear optical material. As for P_2O_5, the amount of Stokes shift is a very large value of 1,320 cm^{-1} although its gain is only about three times that of SiO_2. Utilizing this feature, it became possible recently to use it for fault-point searching of a single-mode optical fiber longer than 100 km for wavelength of 1.59 μm, by using a YAG laser of wavelength 1.32 μm.[7]
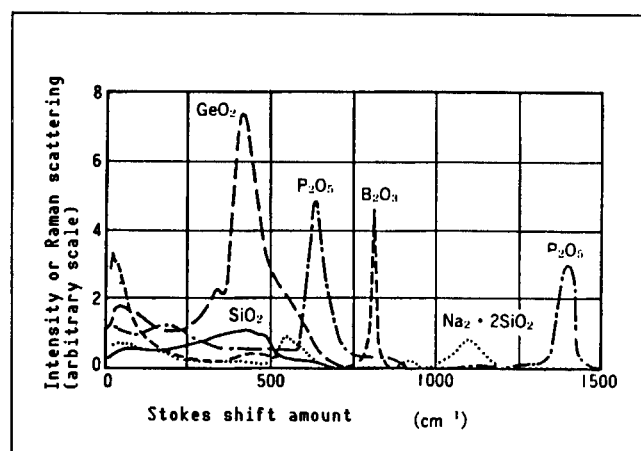

Figure 1. Raman Spectra of Oxide Glasses

Although a clear-cut threshold for stimulated Raman scattering, in a treatment of the forward scattering that neglects the depletion of the excitation light, the following critical input I_{CR} has been obtained as the excitation input at which the powers of the Stokes radiation and the excitation light are equal[3]:

$$\frac{I_{CR}}{A_{eff}} \approx 16 \, \frac{\alpha}{g_R} \tag{1}$$

where A_{eff} is the fiber cross section, α is the loss in the fiber, and g_R is the Raman gain coefficient at the center wavelength. It is assumed that the fiber length is sufficiently longer than $1/\alpha$. For example, if one takes $A_{eff} = 5 \times 10^{-7}cm^2$, $\alpha = 0.4$ dB/km ($9.2 \times 10^{-7}cm^{-1}$), and $g_R = 0.6 \times 10^{-11}cm/W$ (for $\lambda = 1.5 \, \mu m$) for an ordinary single-mode fiber, one obtains a critical input I_{CR} of 1.2 W.

The optical amplification of SRS features a high degree of amplification, a short response time of less than 1 ps, and a relatively high saturation intensity of several hundred mW. In Figure 2(a) is shown a light amplification method by means of SRS.[8] In this method, Q-switched YAG laser pulse with wavelength 1.34 μm is used as an excitation light, and a wavelength-variable fiber Raman laser is used as a signal light. In Figure 2(b) is shown the gain characteristic when using a PANDA-type polarization maintaining fiber, with the excitation input on the abscissa. A PANDA-type fiber is one in which a stress-imparting part is provided on both sides of the core with a separation of about 30 μm to generate birefringence in order to maintain the incident polarization. It can be seen that the gain of the first Stokes radiation with wavelength 1.422 μm increases exponentially as the excitation input is increased. For the excitation input of 0.5 W the gain is 20 dB and the gain coefficient is 0.04 dB/mW. For the second Stokes radiation the gain starts to rise sharply at around the excitation input of 2.2 W, reaching a high gain of about 20 dB at 3.5 W. By focusing the attention on such a high value of the gain, its applications to the amplification of the optical solitons and to the soliton lasers are very actively studied.
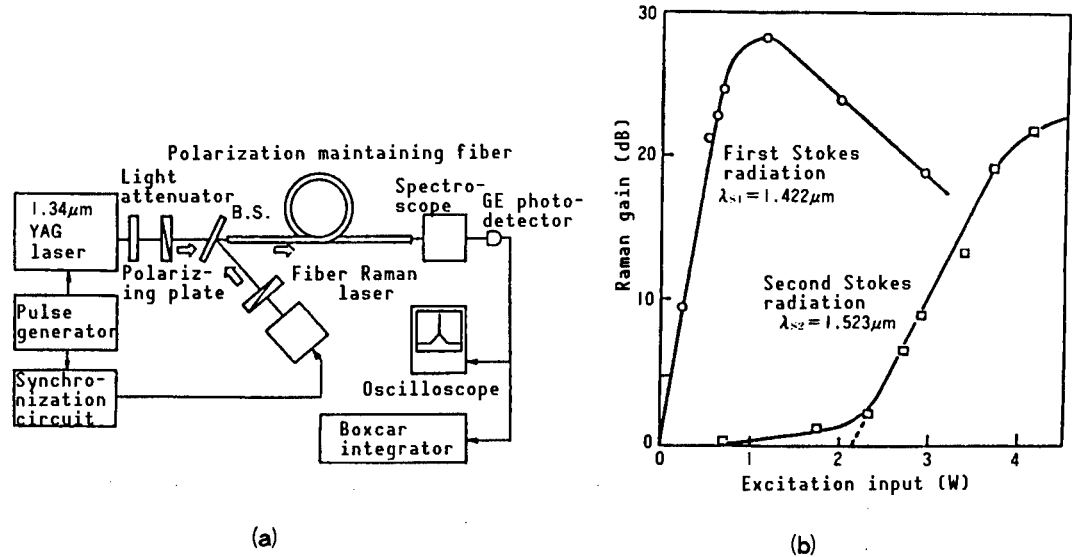

Figure 2. (a) Light Amplification Measuring System by Stimulated Raman Scattering
(b) Dependence on Excitation Input of Raman Gain

16

4. Stimulated Brillouin Scattering

The stimulated Brillouin scattering (SBS) is a scattering of light by the interaction between an excitation light and acoustic phonons, and the nonlinearity of the polarization is caused by the electrostrictive effect. In contrast to the fact that both forward and backward scattering are observable in SRS, backward scattering is generated strongly in SBS because of the momentum conservation law of photons and acoustic phonons.

When the critical input I_{CB} for SBS is defined similarly to that for SRS,[3] it is given by

$$\frac{I_{CB}}{A_{eff}} = 21\frac{\alpha}{g_B} \tag{2}$$

For $A_{eff} = 5 \times 10^{-7}\text{cm}^2$, $g_B = 4.6 \times 10^{-11}\text{cm/W}$ (a value which is about one order of magnitude larger than that of SRS), and $\alpha = 0.4$ dB/km, one obtains I_{CB} of about 2.2 mW. Namely, the critical input I_{CB} is about three orders of magnitude smaller than I_{CR}. Because of this, SBS can readily be generated by letting a semiconductor laser light of spectral line width of several MHz and an output of about 10 mW incident light on a long single-mode fiber.
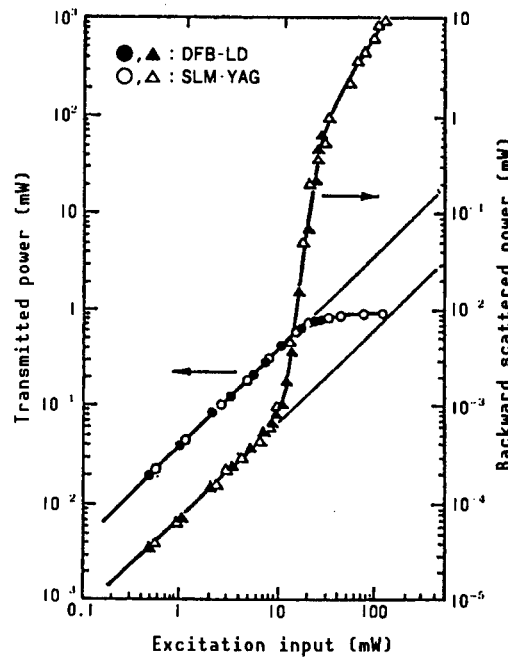

Figure 3. Relationship Between Excitation Input and Backward Scattered Power for Stimulated Brillouin Scattering in 1.3 μm Wavelength Band
DFB-LD means a single-mode semiconductor laser and SLM-YAG means a single-model YAG laser.

17

Figure 3 shows the result of SBS measurement by a single frequency semiconductor laser of wavelength 1.3 μm.[9] For smaller values of the excitation input, the transmitted power increases in proportion to the increase in the excitation light. However, when the excitation input exceeds the critical power of 10 mW for SBS, the reflected wave begins to increase suddenly, and the transmitted power does not increase even when the excitation input is increased further. Recently, there have been reported a laser which oscillates with a threshold of less than 1 mW and a frequency-stabilized laser that utilizes the above-mentioned low threshold. In addition, research is underway to apply SBS to a gyroscope or the narrow-band optical amplification of coherent light.

5. Parametric Optical Mixing

Both SRS and SBS represent resonance effects of light with the phonons of a medium, but there exists an effect that modulates the nonresonant component of $X^{(3)}$, that is, it simply modulates the dielectric constant in a nonlinear fashion. In this case, phenomena based on the nonlinear refractive index such as parametric optical mixing, optical Kerr effect, and the like are given by the real part of $X^{(3)}$.

Parametric optical mixing is also called stimulated four-photon mixing (SFPM).[5] It is a phenomenon in which two excitation photons with frequency ν_p and a Stokes photon with frequency ν_s on an optical fiber generate an anti-Stokes photon with frequency ν_0 that satisfies the relation $\nu_0 = 2\nu_p - \nu_s$, thereby emitting simultaneously a Stokes and an anti-Stokes radiation by stimulation. This phenomenon can be interpreted as follows. A nonresonant lattice vibration is induced in the medium by the beat $\nu_p - \nu_s$ that is generated by the strong electric field E_p of the excitation light and the Stokes electric field E_s. When a wave with frequency ν_p propagates in the medium, an anti-Stokes radiation E_a with frequency $2\nu_p - \nu_s$ modulated by the lattice vibration $\nu_p - \nu_s$ is generated as a sideband wave.

To generate the interaction efficiently, it is necessary to satisfy the strict energy conservation law and the momentum conservation law between the E_a wave and the $E_p{}^2 E_s{}^*$ wave. Namely,

$$\left. \begin{array}{l} 2\omega_p = \omega_a + \omega_s \\ \Delta K = 2K_p - K_a - K_s \\ \quad = 0 \end{array} \right\} \tag{3}$$

For a highly efficient interaction it is important to satisfy the condition $\Delta K = 0$. In the case of an optical fiber, ΔK is the sum of the material distribution due to fiber material and the structure distribution due to structures. In Figure 4 is shown an example of SFPM for an excitation with 1.32 μm light in a single-mode fiber with a core diameter of 7.6 μm.[10] In this case, the amount of Stokes shift is 1,400 cm^{-1} where the wavelength of the Stokes radiation is 1.620 μm and that of the anti-Stokes radiation is 1.114 μm.

6. Generation of Second Harmonic Wave, Sum-Frequency Wave, and Difference-Frequency Wave

These effects originate from the second-order nonlinear effect ($X^{(2)}$), but it is difficult to generate them in an isotropic glass medium having an inversion symmetry. To obtain these effects, a nonlinear material such as $LiNbO_3$, $KTiPO_4$ (KTP), β-BaB_2O_4 (BBO), or the like is usually used. Of these the optical waveguide technique of $LiNbO_3$ by the Ti diffusion method has been established, and waveguides with low loss (less than 0.5 dB/cm) can be manufactured relatively easily. In the second harmonic wave generation using this waveguide, phase matching is done by utilizing the fact that birefringence depends greatly on the temperature. A conversion efficiency of 0.8 percent is obtained for an input fundamental wave of 1.06 μm frequency and a power of 65 mW, which means an enhancement of the efficiency of approximately two orders of magnitude compared with a bulk material.
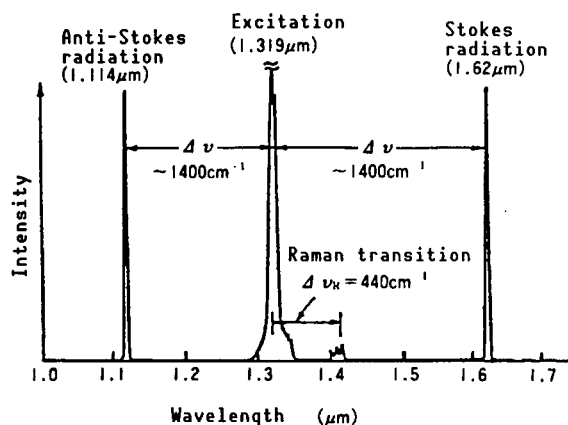

Figure 4. Stimulated Four-Photon Mixing

The proton exchange method is also effective as a waveguide formation technique. In this method, it is possible to form a waveguide with strong confinement of light since the index of refraction of the extraordinary ray can be increased by 1.2~1.4 by Li^+ — H^+ substitution. In addition, the waveguide has a large resistance to light damage. Phase matching between a waveguide mode and an emission mode using Čerenkov radiation generates an optical output of 0.2 mW (efficiency of 1 percent) at a wavelength of 0.42 μm for a 0.84 μm semiconductor laser beam of 20 mW.

Single crystal fibers of $LiNbO_3$ have also been investigated, and a second harmonic wave is obtained with an efficiency of 50 times that of the conventional case for a fiber 25 μm in diameter and 5 cm long. In optical fibers of silica, there are also reports on the generation of a sum-frequency wave and the generation of a second harmonic wave by making strong optical pulses to be incident on the fiber. These are considered to be caused by a gradual generation of color centers caused by a weak second harmonic component generated by the quadrupole moment, which creates a second-order nonlinearity ($X^{(2)}$ diffraction grating) in the fiber.

19

7. Self-Phase Modulation Effect and Optical Solitons

The self-phase modulation effect (SPM) is caused by the Kerr effect, and the refractive index change it causes is represented by

$$\Delta n(t) = \eta_2 \mid E(t) \mid^2 \qquad (4)$$

where $E(t)$ is the electric field and η_2 is the nonlinear refractive index. In the case of a silica optical fiber η_2 is in the order of $3.2 \times 10^{-16} cm^2/W$. If an optical Kerr effect occurs in a short time, the phase of the electric field varies with it. This is SPM and the change $\Delta\omega(t)$ of the angular frequency is given by

$$\Delta\omega(t) = -\frac{\partial}{\partial t}\Delta\phi(t)$$
$$-\frac{2\pi\eta_2 l}{\lambda}\frac{\partial}{\partial t}\mid E(t)\mid^2 \qquad (5)$$

where l is the length of the medium through which the light propagates and λ is the wavelength of the light that generates the electric field. Accordingly, when a high-intensity, ultrashort optical pulse is incident on a fiber, a rapid change in the phase takes place in a short time, and it becomes a pulse whose frequency changes with time (frequency chirping) as shown by equation (5). Namely, as shown in Figures 5(a) and 5(b), the frequency in the leading part of the pulse is lower than the carrier frequency, whereas it is higher in the trailing part of the pulse.
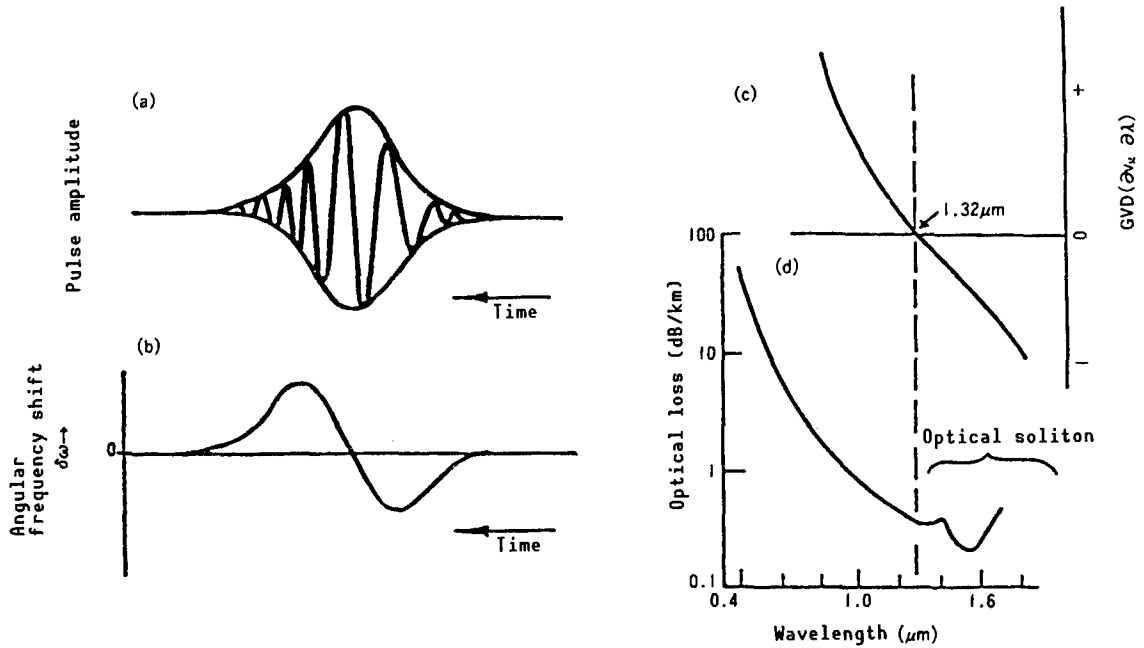

Figure 5. Self-Phase Modulation Effect, Group Velocity Dispersion,
and Loss-Wavelength Characteristic in Optical Fiber

20

Now, let us consider how the waveform changes as a pulse having SPM propagates in a dispersive medium.[1] Single mode silica fiber has a group velocity dispersion (GVD) characteristic as shown in Figure 5(c) and an optical loss-wavelength characteristic as shown in Figure 5(d). A zero dispersion wavelength where the material distribution and the structural distribution are in equilibrium exists in the vicinity of wavelength 1.32 μm, and the GVD becomes positive on its shorter wavelength side while it is negative on its longer wavelength side. Accordingly, when the center wavelength of an optical pulse that has SPM is found in the positive GVD region, the leading part of the pulse is shifted to the long wavelength side so that the velocity of that portion becomes larger, whereas the velocity of the trailing part becomes smaller because the frequency becomes higher. As a result, energy at the central part of the pulse is distributed between both wings, eventually approaching a rectangular wave as shown in Figure 6(a).

(a)   (b)

Amplitude

Time   Time

Positive GVD   Negative GVD (Optical soliton)
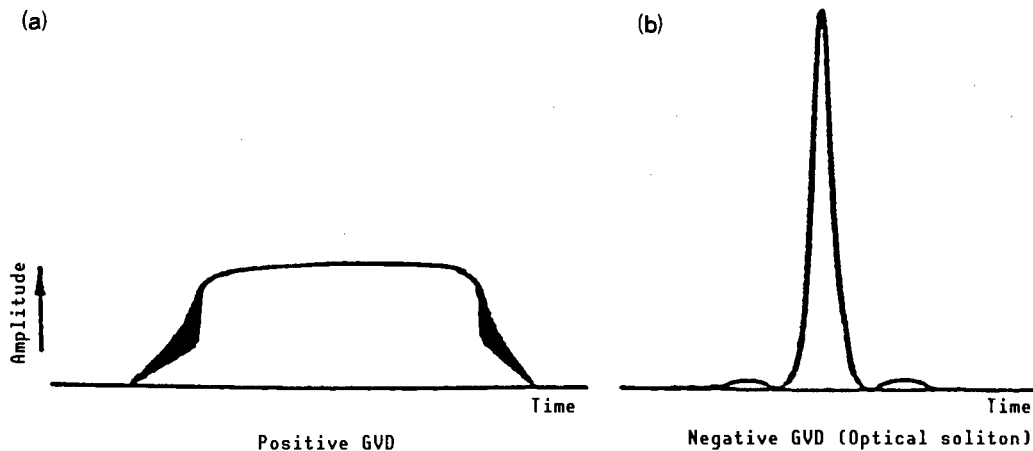
Figure 6. Nonlinear Wave Motion in Optical Fiber
        (a) Case of positive GVD
        (b) Case of negative GVD (corresponding to a soliton)

On the contrary, in a chirp pulse in the wavelength region larger than 1.32 μm where the GVD is negative, the velocity in the leading part of the pulse becomes smaller, and in the trailing part it becomes larger. Consequently, the optical pulse is compressed as shown in Figure 6(b), eventually becoming a narrow stable pulse where the expansion due to GVD and the compression due to SPM are in balance. This is the principle of generation of a soliton.[2,11] What should be noted here is the fact that the negative GVD for which a soliton can be realized occurs in the wavelength region of the least loss in a silica fiber so that it is extremely effective in high-speed, long-range communications.

The equation for describing the envelope soliton in an optical fiber is a nonlinear Schroedinger equation (NLS) which is given by

$$(-i) \frac{\partial u}{\partial q} = \frac{1}{2} \frac{\partial^2 u}{\partial s^2} + |u|^2 u \tag{6}$$

21

where u(q,s) is the soliton wave function, the lowest—order solution to the above equation (the normalized N = 1 soliton) is known to be given by

$$u(q,s) = 2\eta \, sech(2\eta s) \, e^{-i2\eta^2 q} \qquad (7)$$

The initial value problem for NLS has been solved by Satsuma and Yajima, and it is known that the number N of the eigen values for an input optical pulse u(o,s) = Asech(s) satisfies the relation[12]

$$A - \frac{1}{2} < N < A + \frac{1}{2} \qquad (8)$$

Here, N is an integer which represents the order of the normalized soliton. Under the condition A<½, the effect of GVD dominates that of SPM, and it does not correspond to a soliton. The condition for N = 1 soliton is given by

$$\frac{1}{2} < A < \frac{3}{2} \qquad (9)$$

and has the form as given by equation (7). The case of η = ½ in equation (7) represents a standard soliton of N = 1, and its energy ϵ is given by

$$\epsilon = P_o \int_{-\infty}^{\infty} |u|^2 dS = 4\eta \frac{\sqrt{\left|\frac{\partial^2 \kappa}{\partial \omega^2}\right|}}{\kappa \sqrt{Z_o}} \qquad (10)$$

where $\kappa = \frac{1}{2} k_0 n_2$ and $\frac{\partial^2 k}{\partial \omega^2}$ is connected to GVD by the following relation:

$$|D| = \frac{2\pi c}{\lambda^2} \left|\frac{\partial^2 \kappa}{\partial \omega^2}\right| \qquad (11)$$

In equation (10), Z_0 is called normalized propagation distance which is given for a sech pulse with a total half—value width τ_{FWHM} is given by

$$Z_0 = 0.322 \left(\frac{2\pi c}{\lambda^2}\right) \frac{\tau_{FWHM}^2}{|D|} \qquad (12)$$

Further, in the case of a soliton wave, from n_2, $|D|$, A_{eff} for the medium and the incidence pulse width τ_{FWHM}, the peak power P $_{N=1}$ of N=1 soliton with that width is given by

$$P_{N=1} = 0.776 \frac{\lambda^3}{\pi^2 c n_2} \frac{|D|}{\tau_{FWHM}^2} A_{eff} \qquad (13)$$

For example, for τ_{FWHM} = 7 ps, $|D|$ = 16 ps/km/nm, λ = 1.55 μm, and A_{eff} = 1 x 10^{-6}cm^2, one obtains P_{N-1} is about 1 W. By the use of a 1.5 μm band fractional shift fiber for optical soliton, and by further reducing the diameter of the cross section (spot size), it becomes possible to set approximately

$|D| = 2$ ps/km/nm and $A_{eff} = 2 \times 10^{-7}$ cm^2, so that $P_{N=1}$ can be reduced to about 25 mW. Since a semiconductor laser with peak output of several tens of milliwatts is now readily available, the potential for realizing optical communications is fairly high.[13]
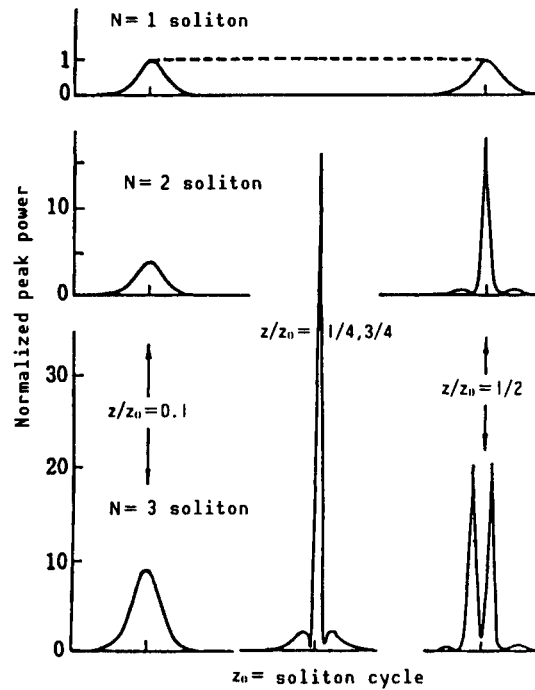

Figure 7. Changes in Waveform of N = 1,2, and 3 Solitons

In Figure 7 are shown the waveform changes for N = 1,2 and 3 solitons. The N = 1 soliton does not change its waveform along the propagation direction as shown by equation (7), and the energy is the lowest, so that it is promising for use in optical communications. As shown in the figure, the higher-order solitons of N = 2 and 3 have a cycle for which the waveform change satisfies

$$q = \frac{\xi}{Z_0} = \frac{\pi}{2} \frac{\xi}{Z_{SP}} = \frac{\pi}{2} \tag{14}$$

In the above equation, Z_{SP} is called soliton cycle, and is given by

$$Z_{SP} = 0.322 \left(\frac{\pi^2 c}{\lambda^2} \right) \frac{\tau_{FWHM}^2}{|D|} . \tag{15}$$

The higher-order soliton may be regarded as the propagation of a plurality of N = 1 soliton while they are interfering. For a certain distance the interference among the solitons is in phase where the solitons strengthen each other, while for another distance they are in opposite phase and weaken each other. In this way, a soliton propagates with its waveform changing for different soliton cycles as shown in the figure.

23

In 1980, Mollenauer at Bell Labs demonstrated the presence of a soliton in a fiber based on the changes of the SHG autocorrelation waveform, as shown in Figure 8, by the use of a 700 m single-mode fiber.[14] According to the figure, an N = 1 soliton is excited at P = 1.2 W, and its pulse width remains the same as that of the input pulse in spite of the presence of GVD for the fiber. By increasing the input peak power to 5W and 11.4 W, it can be seen that the higher-order solitons described above are actually generated.
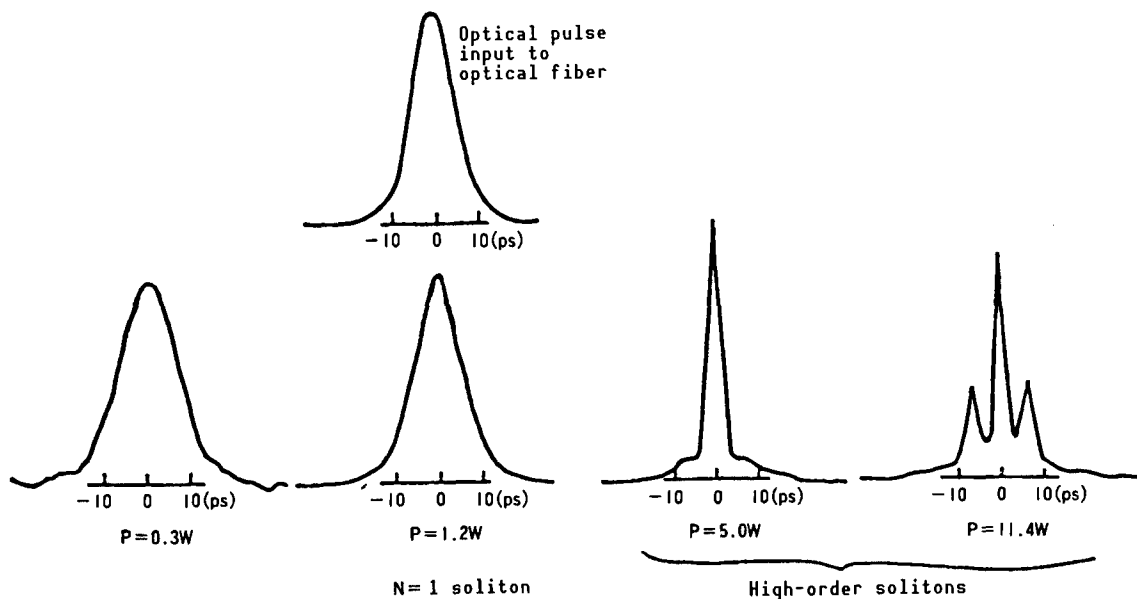
Figure 8. First Experimental Verification of Optical Solitons

8. Optical Soliton Communication

An optical soliton will propagate indefinitely without any waveform distortion in an ideal lossless propagation path, but when a loss exists, the nonlinearity is weakened and eventually it ceases to be a soliton. Although the loss of a silica optical fiber is currently a low value of 0.2 dB/km, the loss becomes a problem when an optical soliton is to be propagated over a distance of nearly 100 km. Namely, in the case of propagation of 50~100 km, the optical loss becomes 10~20 dB so that even when an N = 1 soliton pulse is propagated over such a long filter, the soliton transmission is not possible. Therefore, it becomes necessary to recover the weakened nonlinearity by carrying out one optical amplification.

For the repeating amplification of the soliton, use is made of a direct amplification of light that does not include a conversion to an electrical signal. An optical amplification phenomenon which is of interest in this case is the stimulated Raman scattering described in section 3.[15] In Figure 9 is shown the Stokes wavelength dependence of the SiO_2 Raman gain coefficient. In the case of the Raman gain, the optical fiber loss is compensated for in a manner of distributed constants, and there is realized as a whole an equivalent lossless path.

When the loss of the optical fiber is called Γ and the degree of amplification is g, equation (6) can be rewritten as

$$(-i) \frac{\partial u}{\partial q} = \frac{1}{2} \frac{\partial^2 u}{\partial s^2} + |u|^2 u + i (\Gamma - g) u \qquad (16)$$

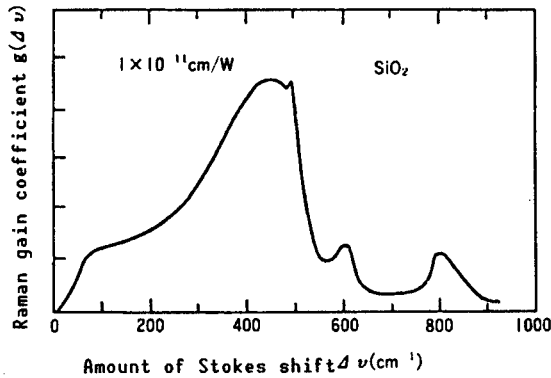
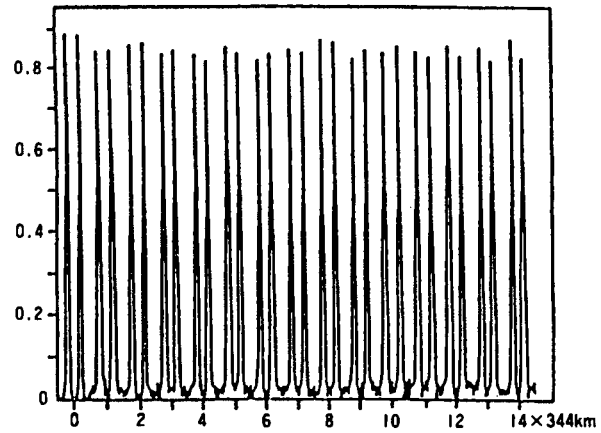Figure 9. Changes of Raman Coefficient of Silica Fiber (SiO₂) Vs. Stokes Shift Amount

Figure 10. Amplified Repeating of Soliton Pair With Pulse Width of 10 ps and Interval of 100 ps by Stimulated Raman Scattering (Result of computation)

Therefore, when the gain g of Raman scattering is equal to the fiber loss Γ, an ideal soliton can propagate in a long fiber.

Using the Raman scattering, Hasegawa showed by computer simulations that a soliton pulse of 10 ps width can stably propagate over 4,800 km.[16] The situation is shown in Figure 10. This represents the result of examining a soliton pair with a pulse width of 10 ps and an interval of 100 ps at every 344 km. Here, $P_{N=1}$ is 30 mW, the loss in fiber is 0.3 dB/km, and the amplifying repeater interval is 34.4 km. Even after a propagation of 4,800 km, it is found that the soliton pair form solitary waves without deformation of the waveforms. When repeated Raman amplifications are given, the noise characteristic becomes a problem. However, one soliton contains a very large number of photons (on the order of 10^6 pieces) so that the transmission with high S/N becomes possible over several thousand km. Mollenauer and Smith showed that an amplified repeating is possible for a distance of more than 6,000 km by letting a soliton with pulse width of 55 ps revolve in a fiber loop 42 km long.[17] Recently, we have proposed an optical amplification by using a fiber doped with a rare-earth element (erbium ion, E_r^{3+}) as a new method of soliton transmission. In this case, a soliton with N = 1.2~1.4, instead of an N = 1 soliton, is input to the fiber, which is a preemphasis method that makes use of the dynamic range of the soliton.[13] By this method, a multiple repeater transmission becomes possible, with amplifiers of a concentrated constant time of several meters long, not the distributed constant type (length of about 40 km) of amplification in the case of SRS. The E_r amplifier is attracting attention as a reliable high-performance method because it has a high degree

of amplification, there is no polarization dependence and no temperature
dependence in the gain characteristic, and the insertion loss is small because
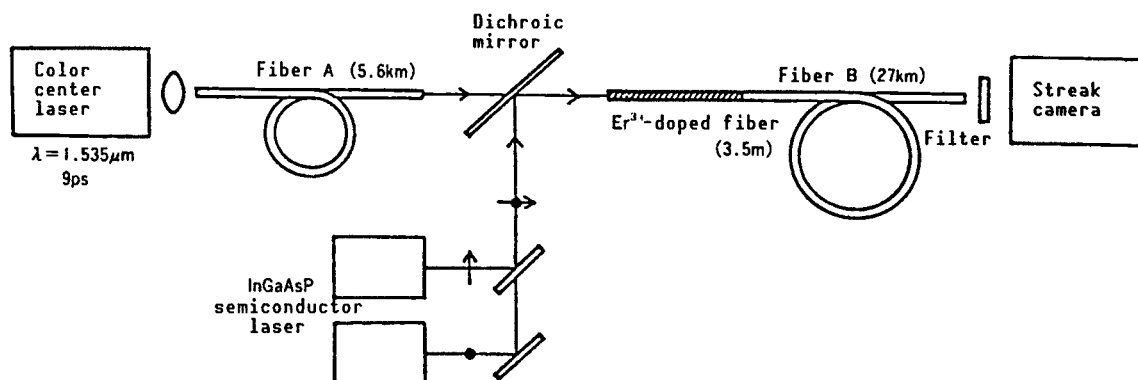it is of in-line type.[18]

Figure 11. Constitution Diagram for Optical Soliton Propagation
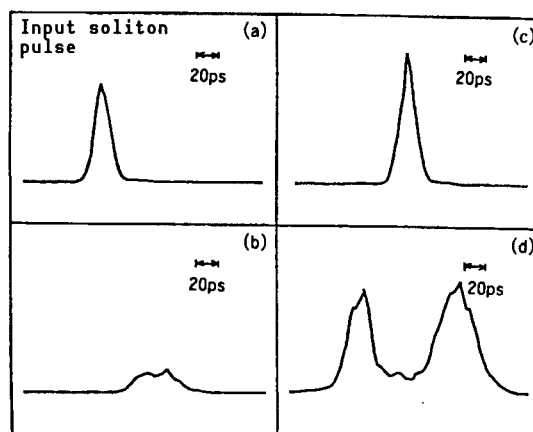by Amplification of E_r^{3+}-Doped Optical Fiber

Figure 12. Propagation of Optical Soliton by an
E_r^{3+}-Doped Optical Fiber

The constitution of soliton transmission by an E_r amplifier is shown in Figure
11.[19] To generate a soliton, a color center laser 1.535 μm long is used, and
the pulse width of the soliton is about 10 ps. The amplitude of the soliton is
diminished after propagation through a fiber A 5.6 km long. However, it is
amplified then by an E_r amplifier, propagated again through a fiber B, and
detected by a streak camera. Figure 12 shows the result. Figure 12(a) is the
waveform of a soliton on fiber A, and Figures 12(b) to 12(d) show soliton
waveforms when the excitation input to the E_r fiber is increased. When the
excitation input is weak as in Figure 12(b), the amplitude of the output
waveform is small, and the output pulse width is spread to 42 ps. This shows
that the amplitude of the optical pulse is spread by GVD since the pulse width
to fiber B is small compared with the soliton level. When the excitation input
is increased, the degree of amplification is increased and becomes as shown in
Figure 12(c). Under this condition, the output width is approximately equal to
the input pulse width, and this is serving as the principle of the preemphasis

method. A waveform analysis on the assumption of a light loss of 0.22 dB/km found that a soliton with A = 1.5 was excited, and it was propagating in fiber B. Since A = 1.5 is used instead of N = 1, the method is called the pre-emphasis method. What is important is that a waveform having a pulse width equal to that of the input is regenerated and relayed. With a further increase of the degree of amplification, the soliton becomes a double-peak type pulse as shown in Figure 12(d). This shows that the higher-order soliton is excited because of the high degree of amplification, with its value of N being 3~4.

9. Summary

The nonlinear optical effects in an optical fiber and their applications to optical communications have been reported. Research in this field that began in the 1970s has produced recent significant results which are now being implemented in various optical technologies. For example, applications of the SRS effect to fault-point searching and optical soliton transmission are quite interesting. Further, the self-phase modulation effect, which becomes the basis for optical solitons, is also playing an important role in the new mode-locking laser technique for generating ultrashort pulses.

This field can be applied also to ultrahigh-speed optical switching so that widespread applications are conceivable to optical information processing including optical computers, and for these reasons further advances are earnestly desired.

References

1.   Nakazawa, M., OYOBUTSURI, General Report, Vol 56, 1987, p 1256.

2.   Hasegawa, A. and Tappert, F., APPL. PHYS. LETT., Vol 23, 1973, p 142.

3.   Smith, R.G., APPL. OPT., Vol 11, 1972, p 2489.

4.   Ippen, E.P. and Stolen, R.H., APPL. PHYS. LETT., Vol 21, 1972, p 539.

5.   Stolen, R.H. and Bjorkholm, J.E., IEEE J. QUANTUM ELECTRON., Vol QE-18, 1982, p 1062.

6.   Nakazawa, M., Nakashima, T., and Seikai, S., APPL. PHYS. LETT., Vol 45, 1984, p 823.

7.   Suzuki, K., Noguchi, K., and Uesugi, N., ELECTRON. LETT., Vol 22, 1986, p 123.

8.   Nakazawa, M., APPL. PHYS. LETT., Vol 46, 1985, p 628.

9.   Aoki, Y., Tajima, K., and Mito, I., CLEO'86, THU 4-1, 1986.

10.   Chinlon Lin, SPIE 355, 1982, p 17.

11. Hasegawa, A., "Optical Solitons in Optical Fiber," "Frontiers of Physics," edited by Y. Otsuki, Kyoritsu Publishing Co., 1988.

12. Satsuma, J. and Yajima, N., SUPPL. PROG. THEOR. PHYS., Vol 55, 1974, p 284.

13. Nakazawa, M., Suzuki, K., and Kimura, Y., J. APPL. PHYS., Vol 66, 1989, p 2803.

14. Mollenauer, L.F., Stolen, R.H., and Gordon, J.P., PHYS. REV. LETT., Vol 45, 1980, p 1950.

15. Mollenauer, L.F., Stolen, R.H., and Islam, M.N., OPT. LETT., Vol 10, 1984, p 3302.

16. Hasegawa, A., APPL. OPT., Vol 23, 1984, p 3302.

17. Mollenauer, L.F. and Smith, K., Proc. OFC'89, Houston, 1989.

18. Nakazawa, M., Kimura, Y., and Suzuki, K., APPL. PHYS. LETT., Vol 54, 1989, p 295.

19. Ibid., K., ELECTRON. LETT., Vol 25, 1989, p 199.

Applications for Electrooptical Devices

906C7517C Tokyo OPTRONICS in Japanese Feb 90 pp 140-147

[Article by Tetsuzo Yoshimura, Fujitsu Research Laboratory]

[Text] 1. **Introduction**

The electrooptical devices that control light with electricity—such as optical switches, optical modulators, and deflectors—together with the all-optical devices that control light with light—are expected to play the central role in future optical systems such as optical switching and optical information processing.[1] Their principle of operation is the Pockel's effect (linear electrooptical effect). This is a phenomenon in which the index of refraction changes in proportion to the voltage applied, being one of the second-order nonlinear optical effects analogous to the optical second harmonic generation (SHG).[2] Since, however, the effect is small in the existing inorganic material such as $LiNbO_3$ (LN), it has been difficult to enhance device performance. What is expected to overcome this difficulty is an organic nonlinear optical material.[3]

The present article will present the application targets of the electrooptical devices, the material performance required for them, the present status of the material performance, and the possibility of improving the performance.
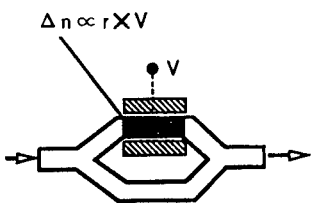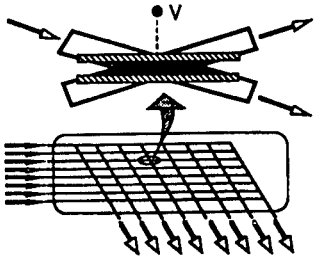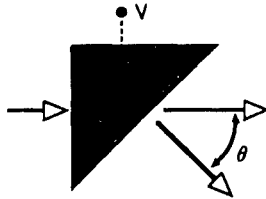
2. **Application Targets and Goals and Performance of Materials**

Table 1 shows the Mach-Zehnder-type optical modulator, total-reflection-type optical switch, and deflector which are typical electrooptical devices.[4] The main application fields may be classified into optical transmission, optical switching, and optical information processing. An ultrahigh-speed optical transmission surpassing several Gb/s uses an external modulation system instead of the direct modulation of the conventional semiconductor laser, which has smaller wavelength variations (chirping) accompanying modulation. The key device here is an electrooptical modulator. In the future, large-capacity, high-speed optical communications that handle dynamic images and high definition pictures will require optical switching without a need for optoelectric conversion, without crosstalk due to electromagnetic induction, and with the possibility of high-speed switching. A high-speed matrix optical

switch is indispensable in this system, along with an optical memory array. This device can also be used as a wavelength control and switching device in the wavelength multiplexing system. These electrooptical devices are expected to be applied not only to optical communications but also to communication between computers, to communication between a computer and a terminal device, and to the optical interconnection within a computer. The deflector is a general-purpose device that makes the dynamic optical interconnection feasible. Its wide range of applications will include, for example, a parallel optical computer, optical printer, and optical disk device. In addition, a spatial optical modulator, variable focusing lens, etc., are important electrooptical devices for the general optical control technology.

Table 1. Goals and Present Performance of Electrooptical Devices

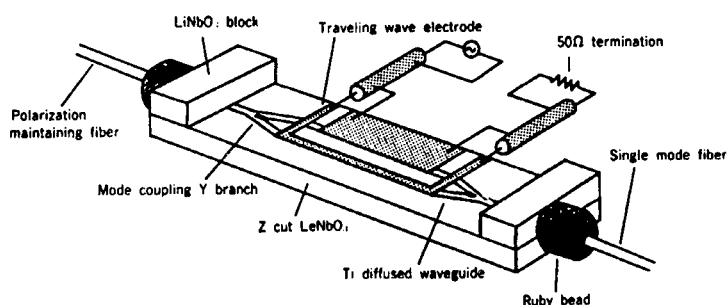| Modulator	Matrix Switch	Deflector
Goal : >10Gb/s	16×16 (100ps)	10-100V >10°
LiNibO₃ : 12Gb/s	8 × 8 (1 ns)	10000V 3°

Figure 1. Ultrahigh-Speed LN Optical Modulator[5]

With these applications in mind, research has been conducted using the most popular electrooptical material, LN. As shown in Table 1, an LN optical modulator for ultrahigh-speed optical transmission has been operated at 12 Gb/s, and a device with a low insertion loss of 2.2 dB has been created

(Figure 1).[5] On the other hand, enormous gaps between current performance and goals remain for the matrix optical switch (SW) and the deflector. This is because the electrooptical coefficient r (which is proportional to the second-order nonlinear electric susceptibility $X^{(2)}$) is so small and the refractive index change Δn (which is proportional to rx voltage) is too large. Therefore, attempts have been made to increase significantly the value of r by using organic nonlinear optical materials.

Figures 2 and 3 show the correlation between the device performance and r for the high-speed matrix optical SW and the deflector. As shown in Figure 2, a limiting line for the high-speed matrix optical SW can be drawn for the switching time and the number of channels (degree of integration) from the conditions on the driving voltage and the device size. Since the modulator is within the limiting line for LN, its performance goals have already been realized. On the other hand, since the high-speed matrix optical SW is outside the limiting line, its goals will be difficult to achieve with LN. If an r value 10 times that of LN can be obtained, then a part of the optical SW goals can be realized, while an r value 100 times that of LN would enable full realization of those goals. Since organic materials can be made into thin film waveguides, and since their r value is large, a marked improvement in the performance of the deflector can be expected. Figure 4 shows the structure of the waveguide-type deflector. A prism-type electrode is formed on a slab-type nonlinear optical waveguide. The application of voltage to this device can generate a prism-type refractive index change, and a light scan with a voltage becomes feasible. The result of an estimation of the deflection angle is shown in Figure 3. It shows that a deflection angle larger than 10° (with an applied voltage of several tens of volts) will be realized if r is 100 times that of LN.
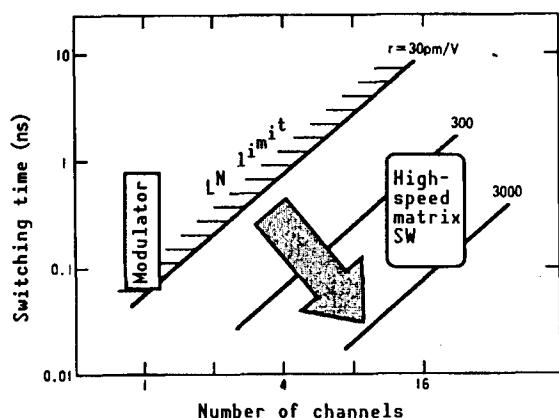

Figure 2. Correlation Between Per-
formance of High-Speed
Matrix Optical Switch and
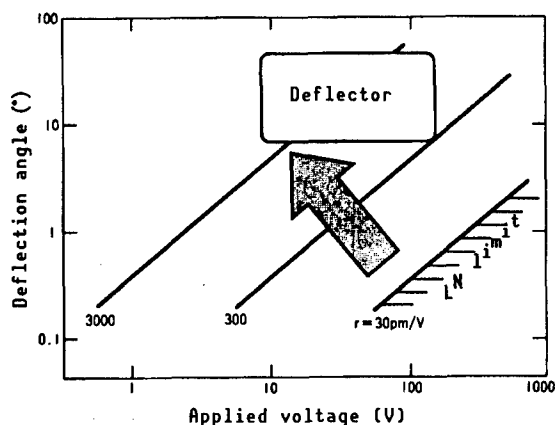Electrooptical Coefficient r

Figure 3. Correlation Between Per-
formance of Deflector and
Electrooptical Coefficient r

From what is said in the above, we have set the first step for the material performance at $r > 10 \times r_{33}$ [LiNbO$_3$] and the second step at $r > 100 \times r_{33}$ [LiNbO$_3$].
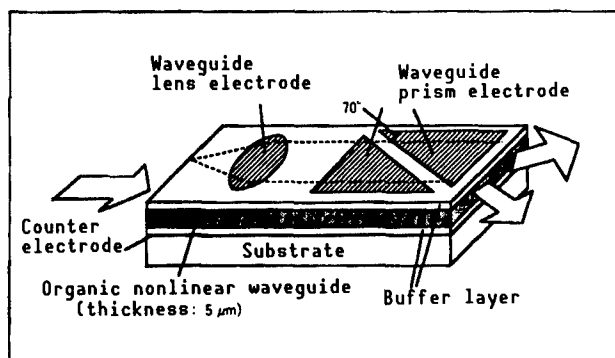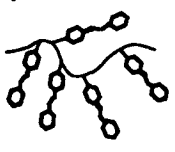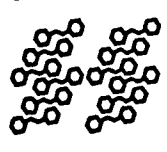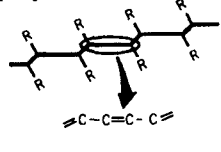
Figure 4. Example of the Structure of Waveguide-Type Deflector
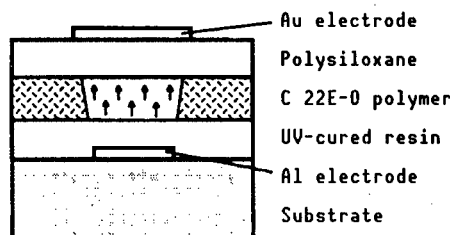
3. Present Status of Material Performance

The electrooptical coefficient r of an organic nonlinear optical material is estimated by using a Mach–Zehnder interferometer[6] or a Fabry–Perot resonator[7] or by converting from the electroreflectance[8] or the phase retardation.[9,10] Using these data, the organic nonlinear optical materials for the electro-optical devices are classified into three groups, and their performances are compared in Table 2.

Table 2. Comparison of Organic Nonlinear Optical Materials for Electro-optical Devices

Electro-optic materials	LiNbO₃	Pendant-attached polymer	Molecular crystal	Conjugated polymer
r (pm/V)	30	20	430	?
Processability	Commercially available	Very good	Poor	Good
Development phase		Device fabrication	Material preparation	Material design

Pendant-Doped Type Polymers

The doped–type polymers are those in which nonlinear optical molecules are added in polymers, and the pendant–type polymers are those in which nonlinear optical molecules are introduced into polymers as side chains. Of these, a pendant–type polymer is shown schematically in Table 2. In either case, a film is formed by spin coating. Then it is softened by heating it to a temperature near the glass transfer temperature, and when the nonlinear optical molecules are oriented by the application of an electric field (poling), an electro-optical effect is generated.

```
              ┌────────┐          ─ Au electrode
         ┌────┴────────┴────┐
         │                  │      Polysiloxane
         │▒▒▒│↑ ↑ ↑ ↑ ↑│▒▒▒│      C 22E-0 polymer
         │                  │
         │      ┌────────┐  │      UV-cured resin
         │──────┴────────┴──│    ─ Al electrode
         │· · · · · · · · · │
         │· · · · · · · · · │      Substrate
         └──────────────────┘
```

Directional coupler   Traveling wave-type modulator

Element length: 3.8 cm   Element length: 3 cm
Crossing angle: 3 degrees   Band: About 1 GHz
Voltage: About 60 V
(Wavelength: 830 nm
Loss <1 dB/cm (slab-type waveguide))

Figure 5. Electrooptical (E-O) Device Using a Pendant-Type Polymer[11]
           Poling between the upper and lower electrodes forms a
           nonlinear waveguide having an electrooptical effect.
           The same electrodes are used for driving the device.

These materials are being studied actively at Bell Labs, Lockheed Corp.,
Hoechst-Celanese Co., etc.[6,11,12] Because film formation is easy, the formation
of waveguides with low loss is possible, the dielectric constant is low, and
speed-matching between the microwave and light is high, trial fabrication of
such devices as optical switches and optical modulators shown in Figure 5 has
been reported.[11] However, the application of these materials to the matrix
optical SW or deflector is difficult because the density of the nonlinear
optical material in the film is low, the molecules cannot be oriented suffi-
ciently because of restrictions on the poling voltage, and the electrooptical
coefficient r obtained is small compared to that of LN, at present.

Methods to offset these problems include the use of liquid crystal polymers or
a forced orientation of the molecules that utilizes the interaction between
the guest (nonlinear optical molecules) and the host (polymers), as developed
by Miyata, et al., at Tokyo University of Agriculture and Mechanics.[13] In
particular, the forced orientation is considered to be a promising approach
because the SHG efficiency surpasses that of MNA (2-methyl-4-nitroaniline) for
several combinations, such as p-nitroaniline as the guest and polyethylene
oxide as the host.[13]

Low-Molecular-Weight Single Crystals

The low-molecular-weight single crystals have a high density of nonlinear
optical molecules, making possible a satisfactory orientation by properly
adjusting the intermolecular interaction within the crystal. An electrooptical
coefficient about 14 times that of r_{33} of $LiNbO_3$ has been obtained in styryl-
pyridiniumeyanine dye (SPCD),[9,10] clearing the first step for r. The limitations
of SPCD are the difficulty of using it to form a waveguide and the large
scattering loss.

In contrast, 4'−nitrobenzylidene−3−acetoamino−4−methoxyaniline (MNBA)[14] developed by Toray has a large value for r which is about 10 times that of LN, and moreover, stability of crystals due to intermolecular hydrogen coupling and marked enhancement of workability have been accomplished for it. Since it has already been used to form a waveguide, this material is considered extremely promising.[15,16]

However, the performance of low−molecular−weight single crystals is limited from above by a value of r which is on the order of 10 x 4 [LiNbO$_3$], so that introducing longer molecules is necessary to improve the performance.

Long-Chain-Type Conjugate Polymers

A representative by this category is polydiacetylene.[17-20] So far, these materials have been studied as third−order nonlinear optical materials, so their evaluation as electrooptical materials is not available yet. Nonetheless, they are considered promising since they have a long and broadly expanded π electron conjugate system and their electronic states can be controlled to a large extent.

In summary, the current trends in developing electrooptical materials are to deal with the first step of r = 10 x r_{33} [LiNbO$_3$] by the low−molecular−weight single crystals, and the second step of r = 100 x r_{33} [LiNbO$_3$] by long−chained conjugate polymers. In addition, it is expected that the characteristics of the pendant−doped−type polymers can be improved by the guest/host interaction and the forced orientation with liquid crystal polymers.

4. Possibility of Enhancing Material Performance

As mentioned above, introducing long−chained conjugate polymers promises a marked enhancement of the electrooptical effect. With this in mind, the following will present the result of investigation by computer simulations of long−chained polymers of polydiacetylene structure using the Austin model 1 (AM1) of molecular orbital method.[21-23]

4.1 Electrooptical Effect of Long-Chained Conjugate Polymers

As shown in Figure 6, r is given approximately by the product of the oscillator strength f and the difference of the dipole moments P_e-P_g between an excited state and the ground state. For this short paper, we studied under the two−level situation, dealing with the ground state and only one of the excited states. The value of f increases with the overlap of the wave functions of the ground state and the excited state, and P_e-P_g increases with the deviation of the wave functions. Accordingly, the basic concept for material design is to optimize r through control of the wave functions. Figure 7(a) shows schematically the relations between the forms of the wave functions and r, f, P_e-P_g increases. Since r is the product of both, r can be increased by generating wave functions that have an intermediate deviation.

34

(a)
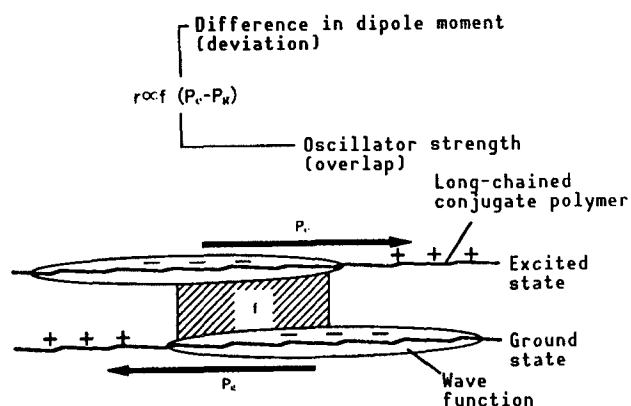

DA34

DAAD34

DADA34

DDAA30

(b)

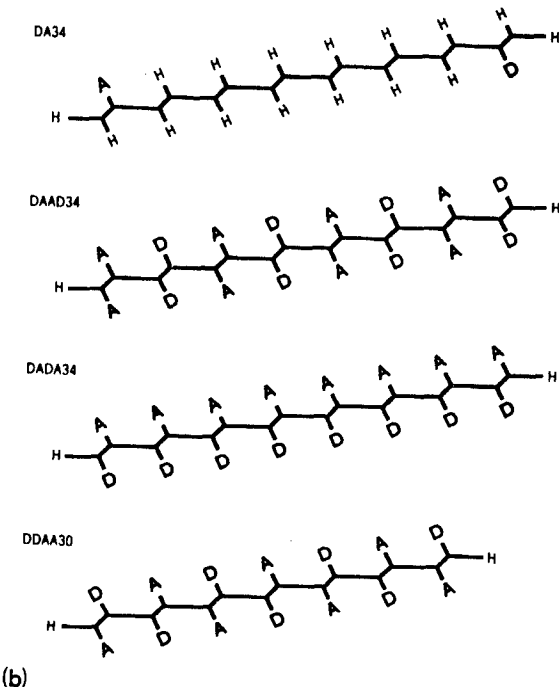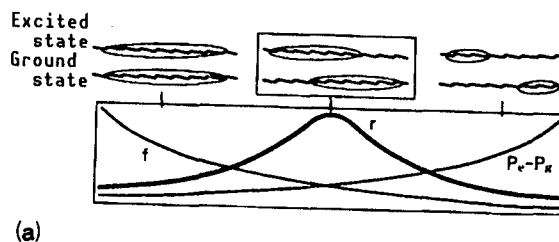Figure 6. Material Design Concept for Increasing Electro-optical Coefficient

Figure 7. Optimizing the Electro-optical Coefficient by Controlling Wave Functions

The next problem is how to adjust the wave functions. Figure 7(b) shows a method in which an acceptor (A: NO_2) that pulls the electron and a donor ($DiNH_2$) that expels the electron are added in various configurations. Here, DA, DAAD, DADA, and DDAA show possible positions for the donors and the acceptors. The numeral following each designation represents the number of carbon atoms in the main chain. The length of 34 carbon atoms corresponds to a molecular length of 42 Å.

Based on these ideas, computer simulations of r were created; the result is shown in Figure 8. Here, the conversion between the second-order nonlinear molecular polarizability β and r is based on the assumption that the molecules are packed with each molecule perfectly oriented. A comparison with the molecular length of 42 Å shows that r is the largest for DAAD. This is because the intermediate deviation for wave functions shown in Figure 7(a) is realized in this configuration.[21] Further, the value of r for each molecule varies according to the molecular length. This is because the balance between the expanse and the deviation of wave functions varies with molecular length.
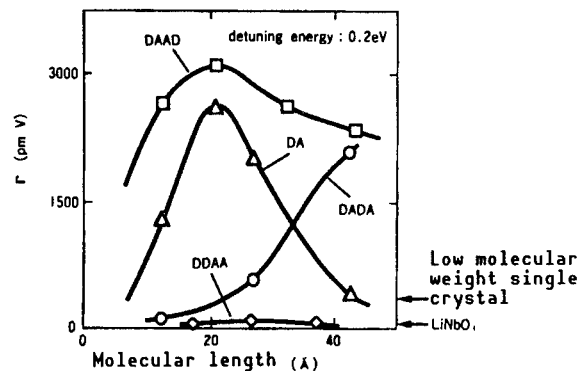
Figure 8. Electrooptical Coefficient of Long-Chain-Type Conjugate Polymers
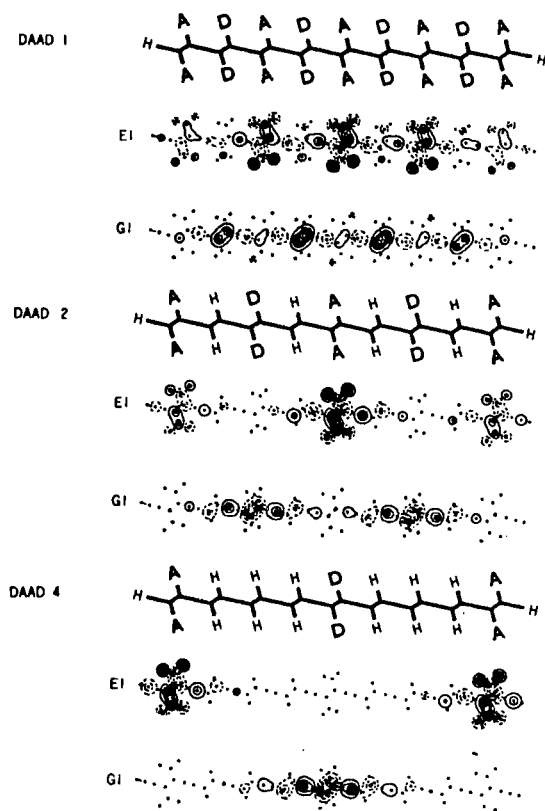

Figure 9. Long-Chain-Type Conjugate Polymers With Various Distances Between D-D and A-A Pairs

G1 represents the highest occupied molecular orbital (HOMO) and

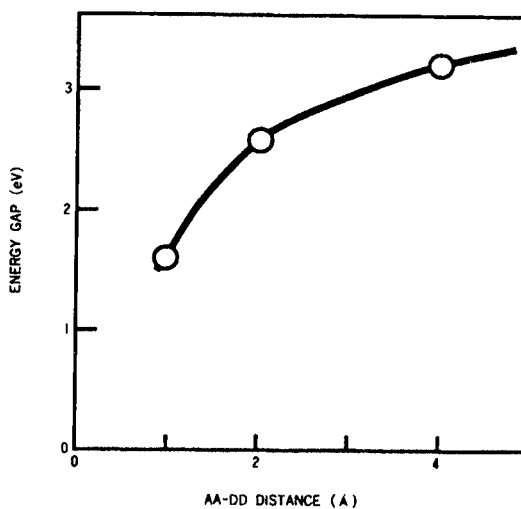E1 represents the lowest occupied molecular orbital (LOMO)

Figure 10. Dependence of Energy Gap on the Distance Between D-D and A-A Pairs

36

This is because the balance between the expanse and the deviation of wave functions varies with the molecular length. A similar dependence on the molecular length has also been reported for the long-chained polyethylene in which one each of the donor and the acceptor is added to each end of the molecule.[24] As is clear from Figure 8, the largest value of r = 3,000 pm/V, namely, 100 times that of LN, is achieved in DAAD.[21] This suggests the possibility of achieving the second step, which will bring about a significant spreading effect in the optical control technology.

4.2 Control of Energy Gap

To increase the nonlinear optical effect, resonant enhancement is effective.[25] In utilizing this it is important to control the energy gap of the nonlinear optical substance. An example will now be presented. In a molecule of the DAAD type, the energy gap will be diminished by short-distance charge motion between the adjacent A-A and D-D pairs.[22] Therefore, controlling the energy gap control should be possible if the charge transfer distance is adjusted by varying the distance between the pairs as shown in Figure 9. As shown in Figure 10, the energy gap is with the increase in the distance between pairs, approaching that of a hydrogen-substituted molecule.[23] Further, a fine adjustment should be possible by controlling the strength (types) of the donor and the acceptor.
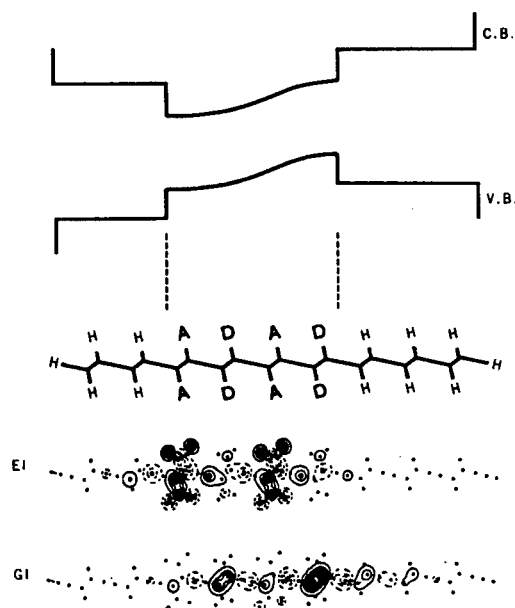

Figure 11. Quantum Well Structure in a Long-
Chain-Type Conjugate Polymer

4.3 Utilization of Multiple Quantum Well Structure

Using the energy gap control mentioned above, it is possible to construct a quantum well structure in a long-chain-type conjugate polymer as shown in Figure 11.[23] The portions where the A-A pair and D-D pair are added is the

well, and the hydrogen—substituted portions are the barriers. From the molecular orbital it can be seen that an electron confinement is actually taking place in the vicinity of the well. The value of r for this quantum well structure is calculated to be about 110 times that of LN; its performance is comparable to that of the DAAD[18] molecule having similar donor—acceptor configuration and an r value about 100 times that of LN.[21] In other words, the above quantum well structure is equivalent to a structure obtained by inserting a DAAD molecule in a hydrogen—substituted polymer chain.
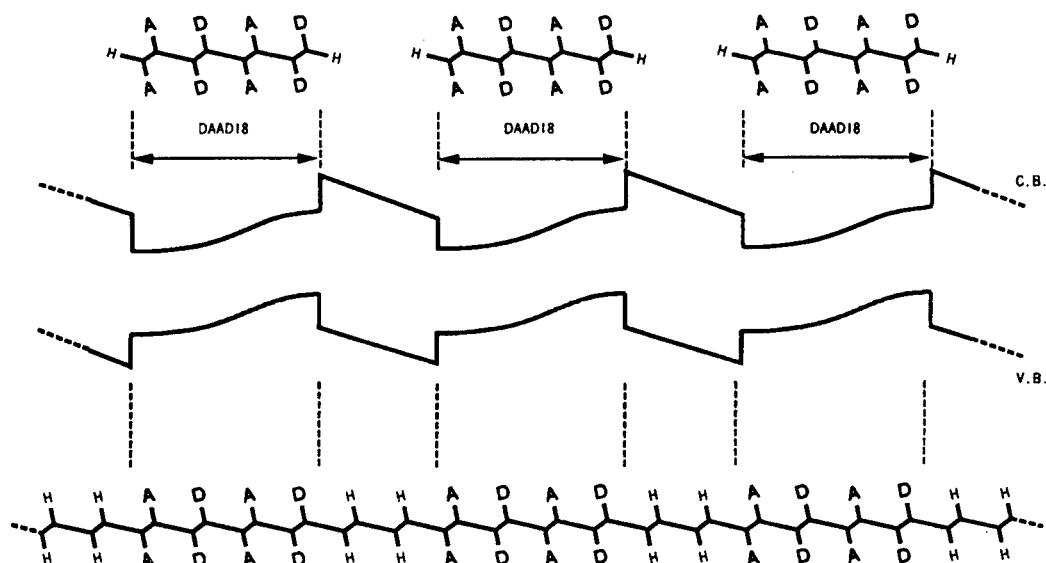

Figure 12. Multiple Quantum Well Structure in
Long—Chain—Type Conjugate Polymer

By multiplying the structure as shown in Figure 12 it is possible to obtain a multiple quantum well structure. This may be regarded as a compact system of DAAD[18] molecules that may be the ultimate form of organic nonlinear optical materials. On the other hand, it is also possible to relax the strength of the electron confinement and give the structure nonlocalizability by decreasing the difference between the energy gaps of the well and the barrier or the width of the well. It should also be noted that the one—dimensional super-lattice is effective for enhancing not only the second—order but also the third—order nonlinear optical effect.

5. Research Direction and Tasks for the Future

From what has been said, there remain the following three goals for the direction of future research in organic materials for electrooptical devices.

Forced Orientation in Pendant-Doped-Type Polymers

To aim at achieving a performance comparable to that of low—molecular weight single crystals, performance should be enhanced through forced orientation by using guest/host interaction or liquid crystal polymers.

Formation of Devices With Low-Molecular Weight Single Crystals

This represents an approach aimed at attaining the first step. The tasks involved are 1) reduction of loss and realization of a single mode for organic waveguides and 2) orientation control and area increase of the crystals and the electrode wiring method. It is necessary to solve these problems by embedding the waveguide in a dielectric, improving crystal growth, etc.

Marked Enhancement in Material Performance by Long-Chain-Type Conjugate Polymers

This is an approach aimed at the eventual performance. The tasks in this area can be concentrated on the control of adding positions of the donors and acceptors and the method of manufacturing one-dimensional superlattices.

6. Summary

1. An optical modulator, high-speed matrix optical switch, and deflector were selected as the application targets. An optical modulator can be realized for the value of r which is on the order of that of LN. To achieve a high-speed matrix optical switch and a deflector it is necessary to have an electro-optical coefficient in the range from $r = 10 \times r_{33}$ [LiNbO$_3$] (first step) to $r = 100 \times r_{33}$ [LiNbO$_3$] (second step).

2. The first step can be handled by using existing low-molecular weight single crystals. It seems that it could also be accomplished by using forced orientation in the pendant-doped type polymers. On the other hand, no existing materials can satisfy the second step; therefore, material development is needed. The strongest candidates for this purpose are considered the long-chain type conjugate polymers, including polydiacetylene.

3. It may be possible to attain the second step, which is to obtain a performance of about 100 times that of LN, by "optimizing the wave function deviations" by using the donors and the acceptors.

4. The energy gap of a long-chain type conjugate polymer can be controlled by adjusting the adding positions of the donors and the acceptors, and the formation of a quantum well becomes possible. The multiple quantum well structure (an array of a large number of quantum wells) may also be regarded as a high-density packing of nonlinear optical molecules of perfect orientation; this may be considered the ultimate form of the organic nonlinear optical material.

5. The three principal tasks for the future will be the forced orientation of pendant-doped type polymers, formation into devices by the use of low-molecular weight single crystals, and a marked increase of the material performance by using long-chain type conjugate polymers.

References

1.   Yoshimura, Fifth Lectures on Ultimate Materials (High Polymer Society), 17 June 1988.

2.   Kobayashi, OYOBUTSURI, Vol 57, 1988, p 174.

3.   Springer Proceedings in Physics, Nonlinear Optics of Organic and Semiconductors, edited by T. Kobayashi, Springer-Verlag Berlin, 1989.

4.   Hiroshi, Nishihara, et al., OPTICAL IC (Ohm-sha).

5.   Seino, M., Mekada, N., Namiki, T., and Nakajima, H., ECOC '89 ThB22-5.

6.   Singer, K.D., Kuzyuk, M.G., Holland, W.R., Sohn, J.E., Lalama, S.J., Comizzoli, R.B., Katz, H.E., and Schilling, M.L., APPL. PHYS. LETT., Vol 53, 1988, p 1800.

7.   Kobayashi, T., Springer Proceedings in Physics, Nonlinear Optics of Organic and Semiconductors, edited by T. Kobayashi, Springer-Verlag Berlin, 1989, p 140.

8.   Nishikawa, Ishikawa, and Koda, 36th Joint Meeting of Societies Related to Applied Physics, Spring 1989, paper 1p-C-1.

9.   Yoshimura, T., J. APPL. PHYS., Vol 62, 1987, p 2028.

10.   Yoshimura, T. and Kubota, Y., Springer Proceedings in Physics, Nonlinear Optics of Organic and Semiconductors, edited by T. Kobayashi, Springer-Verlag Berlin, 1989, p 222.

11.   Lytel, R., Lipscomb, G.F., Stiller, M.A., Thackara, J.I., and Ticknor, A.J., Proc. SPIE 971, 1988, p 218.

12.   Demartino, R., Haas, D., Khanarian, G., Leslie, T., Man, H.T., Riggs, J., Sansone, M., Stamatoff, J., Teng, C., and Yoon, H., Mat. Res. Soc. Symp. Proc., Vol 109, Nonlinear Optical Properties of Polymers, edited by A.J. Heeger, J. Orenstein, and D.R. Ulrich, MRS, Pittsburgh, 1988, p 65.

13.   Watanabe, Miyata, and Miyazaki, Spring Meeting of Japan Society of Applied Physics, 1988, paper 301-A6.

14.   Tsunekawa, Gote, and Iwamoto, 36th Joint Meeting of Societies Related to Applied Physics, Spring 1989, paper 2a-G-8.

15.   Fukuda, Goto, Matagi, Tsunekawa, and Iwamoto, 50th Meeting of Japan Society of Applied Physics, Fall 1989, paper 28a-ZP-6.

16. Gotoh, T., Tsunekawa, T., Kondoh, T., Fukuda, S., Mataki, H., Iwamoto, M., and Maeda, Y., Preprints of International Workshop on Crystal Growth of Organic Materials (CGOM), edited by S. Miyata, 1989, p 234.

17. Tokuta, SOLID PHYSICS, Vol 20 No 11, 1985, p 845.

18. Tanaka, H., Inoue, M., and Hanamura, E., SOLID STATE COMMUN., Vol 63, 1987, p 103.

19. Sauteret, C., Hermann, J.P., Frey, R., Pradere, F., Ducuing, J., Baughman, R.H., and Chance, R.R., PHYS. REV. LETT., Vol 36, 1976, p 956.

20. Thakur, M., Verbeek, B., Chi, G.C., and O'Brien, K.J., Mat. Res. Soc. Symp. Proc. 109, Nonlinear Optical Properties of Polymers, edited by A.J. Heeger, J. Orenstein, and D.R. Ulrich, MRS, Pittsburgh, 1988, p 41.

21. Yoshimura, PHYS. REV., Vol B40, 1989, p 6292.

22. Ibid., APPL. PHYS. LETT., Vol 55, 1989, p 534.

23. Ibid., PACIFICHEM '89, Photonics in Polymers.

24. Morley, J.O., Springer Proceedings in Physics, Nonlinear Optics in Organic and Semiconductors, edited by T. Kobayashi, Springer–Verlag, Berlin, 1989, p 86.

25. Yoshimura, T., OPT. COMMUN., Vol 70, 1989, p 535.

SOR Lithography Used for 0.2 Micron Device

[Article by Toa Hayasaka, chief research worker, LSI Laboratory, NTT: "Paving the Way to Realization of ULSI Exceeding 100M Bits With SOR Lithography"]

[Text] This laboratory is conducting R&D on SOR (Synchrotron Orbital Radiation) lithography as a technique for minute pattern formation on next-generation super LSI. It has been developing an SOR rays generation device which generates highly intense and parallel SOR rays suitable for exposure of superminute patterns of about 0.2 µm which far surpasses 0.5 µm which is said to be the limit of the minute patterns by present ultraviolet ray exposure. This lab was the first in the world to take out SOR rays by a superconducting small storage ring. It further confirmed the effectiveness of SOR lithography by manufacturing approximately 0.2 µm minute pattern semi-conductor devices using SOR rays after developing related devices such as X-ray masks and exposure devices.

What Is SOR Lithography?

SOR lithography is a technique to form an LSI pattern by exposing the pattern on an X-ray mask to a silicon substrate wafer using the soft X-rays in the SOR rays. The wavelengths of the soft X-rays are shorter than those of ordinary X-rays.

Micronization and high integration of LSI sharply enhance operation speed and allow greatly reduced power consumption. Furthermore, high integration of LSI results not only in miniaturization but also various functions for communication devices.

Micronization and high integration of LSI require micronization of processing dimensions. With the ultraviolet ray exposure technique, the main technique at present, pattern dimensions of approximately 0.5 µm are thought to be the limit of micronization because of ultraviolet ray wave-lengths.

To realize super LSI which exceeds 100M bits, micronized patterns of approximately 0.2 µm must be exposed. This has come to require a new exposure technique.

SOR rays are radiated in the tangential direction from electrons when electrons accelerated nearly to the velocity of light are bent by a magnetic field. They are strong parallel X-rays suitable for exposure of micronized patterns. As shown in Figure 1, exposure onto a wafer is done with an X-ray mask which is an LSI pattern formed on a substrate, which transmits soft X-rays well with a metallic material which absorbs soft X-rays well. The SOR rays irradiated onto the X-ray mask generates shades of the LSI pattern depending on the presence or absence of an absorber on the mask. Shades of these SOR rays are transcribed to the resist (photosensitive material) applied to the wafer to become an LSI pattern.

X-ray mask
(section)

SOR rays
(soft X-ray
components)

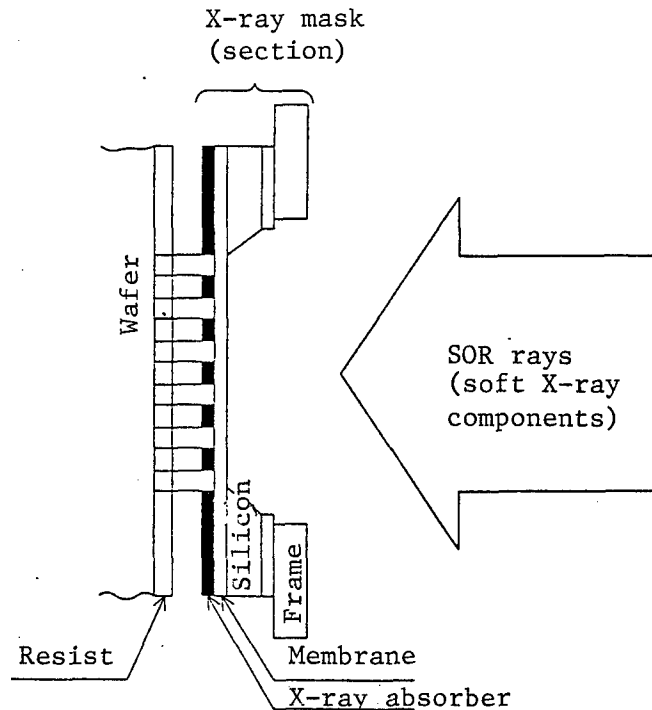Wafer

Silicon

Frame

Resist

Membrane

X-ray absorber

Figure 1. Principle of SOR Lithography

This laboratory confirmed that SOR lithography is a promising technique which breaks the limit of the present ultraviolet-ray exposure technique with the radiated rays experiment of the High Energy Physics Laboratory, Ministry of Education, Tsukuba. However, the conventional SOR ray generation equipment is a huge component for physical research; it is not suitable for industrial use such as LSI manufacturing. Therefore, since 1984 this laboratory has taken the realization of a smaller SOR ray generation device as the main subject for study and began development of a smaller and more economical SOR ray generation device using superconducting magnets.

Smaller SOR Ray Generation Device

The SOR ray generation device uses the principle that the directions of accelerated electrons are bent in a magnetic field. This property allows

construction of a circular orbit which closes at the end of one round, with multiple magnets arranged in a ring. The electron storage ring is the device that causes electrons to continue to revolve in this orbit. A magnet which bends the direction of traveling electrons is called a deflecting magnet and SOR rays are generated here. Figure 2 shows the structure of the super-conducting small storage ring.

To make electrons revolve in orbit, not only deflecting magnets but also four-pole magnets for control are needed to make electrons converge. If the setup precision of these magnets is bad, the electron orbit control for making electrons revolve is impossible. Therefore, magnets weighing from several tons to several tens of tons must be set up at ±0.2 mm or lower precision. If electrons collide with gas molecules, they change their traveling direction and disappear, thus the revolving orbit of electrons must be kept at a superhigh vacuum. The degree of vacuum of this vessel must be better than 10^{-9} Torr (1 Torr = 1 mmHg) which is approximately equivalent to the degree of vacuum of the orbit of an artificial satellite. If a revolving electron emits light, it loses energy. This lost energy is resupplied by the high-frequency electric field generated by microwaves.

The SOR ray generation device is a combination of individual techniques, such as those related to control magnets, vacuums, and high-frequency waves so as to make electrons revolve stably. The ring is operated remotely by computer.

The SOR ray generation device consists of a linear accelerator, an ordinary conducting accelerator ring, and a superconducting small storage ring. Figure 3 shows their layout. This generator has a structure that can take out SOR rays 1) after accelerating and storing the electrons which were accelerated by the first-stage accelerator and made directly incident on the accelerator ring or storage ring or 2) after reaccelerating by the accelerator ring and storing in the storage ring the electrons accelerated by the linear accelerator. Photograph 1 [not reproduced] shows the superconducting small storage ring.

Superconducting magnets are used for the deflecting magnets which bend the traveling directions of the electrons in the storage ring. In a magnetic field, electrons bend while moving in circular orbits, and the radii of the orbits become smaller in inverse proportion to the intensity of the magnetic field. Therefore, orbit radii were made smaller by using superconducting magnets which yield strong magnetic fields twice as strong as those obtained by ordinary electromagnetic magnets using copper wire. As a result, the length of the entire orbit was as small as 1/10 or less of the length of the ring of the radiated rays experiment of the High Energy Physics Laboratory. The size of the storage ring is approximately 2.5 m x 8 m.

Since with a superconducting magnet, current is made to flow across the superconducting wire coil whose electric resistance is zero, power require-ment also becomes almost zero, making low running cost expected. Furthermore, coils of superconducting magnets were provided with an iron yoke with magnetic poles instead of being left air-core. Since this structure forms magnetic circuits with the iron yoke and reduces magnetomotive force, the power supply
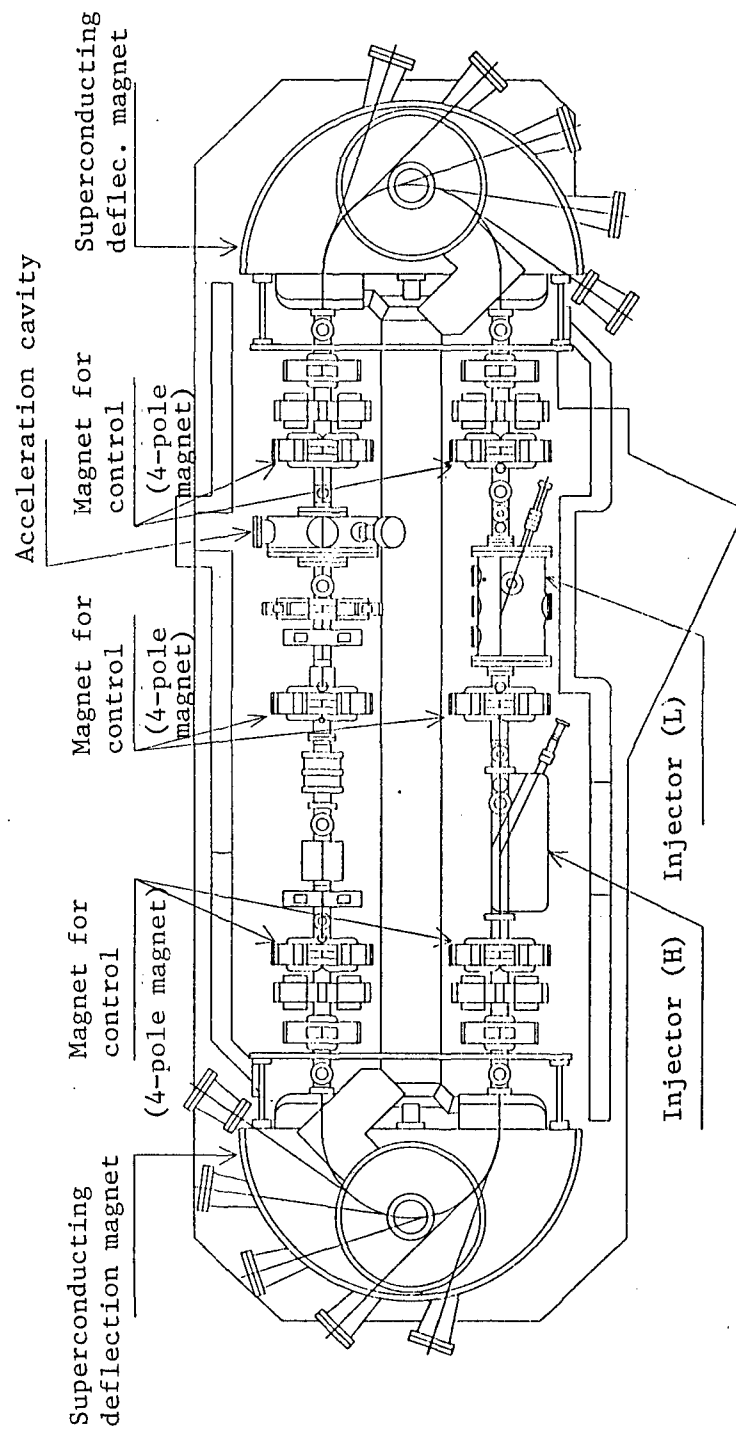
Figure 2. Structure of Superconducting Small Storage Ring

45

for current across coils can be made smaller. In addition, the iron magnetic pole shape was contrived so as to make it possible to secure a wide uniform magnetic field area necessary for revolving electrons. The storage ring has a race track shape and uses two such superconducting magnets; electrons are bent 180 degrees with one of these superconducting magnets. To take out SOR rays, five ports have been provided for one deflecting magnet and 10 ports in total. The largest energy stored is 600 MeV and the power of the rays generated has been designed to reach a maximum level at a wavelength of 7 Å which is suitable for transcription of LSI patterns. Figure 4 shows wavelengths of SOR rays.
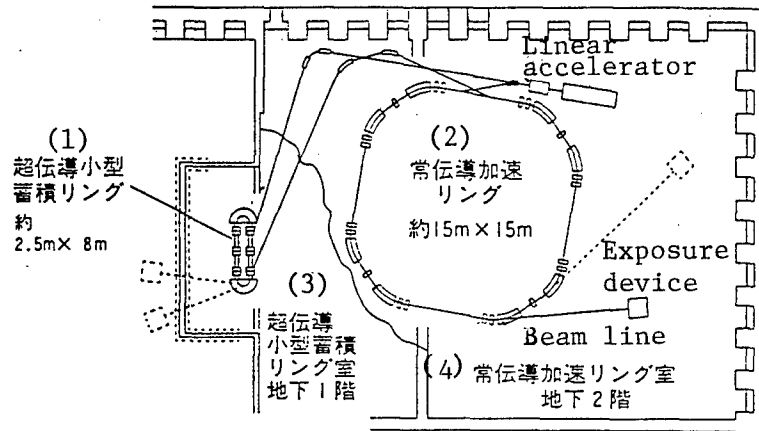

Figure 3. Outline of NTT SOR

Key:
1. Superconducting small storage ring about 2.5m x 8m
2. Ordinary conducting accelerator ring about 15m x 15m
3. Superconducting small storage ring room on basement 1
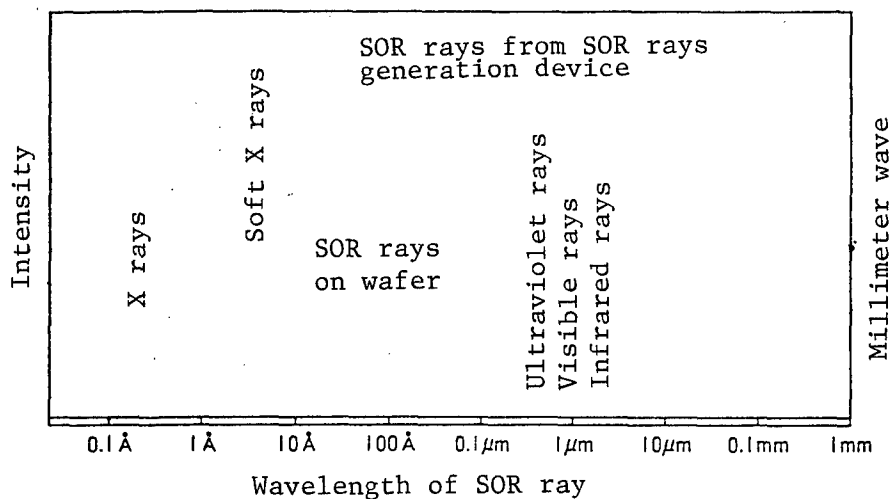4. Ordinary conducting accelerator ring room on basement 2

Figure 4. Spectrum of SOR Rays and Wavelengths Used in Lithography

46

The storage ring of this laboratory has adopted the structure that allows investigation of the possibility of the in-ring accelerating method which reaccelerates and stores in the ring the low energy electrons made incident on the ring from a short linear accelerator. Therefore, the storage ring is provided with the function of accelerating electrons. Realization of this in-ring accelerating method leads to reduction of not only price but also floor area. Since low energy electrons have a short life, they must be made incident in a short time. Therefore, the linear accelerator has been structured so as to be able to take out large current (250 mA) of uniform energy. The ordinary conducting accelerator ring which has been set up in the central part of the layout shown in Figure 3 was developed to supply the storage ring with high-energy electrons but will also play the role of an experimental device of the in-ring accelerating method. In addition, the ring functions as a storage ring so that it can also be used as an SOR rays generation device if in-ring acceleration is realized.
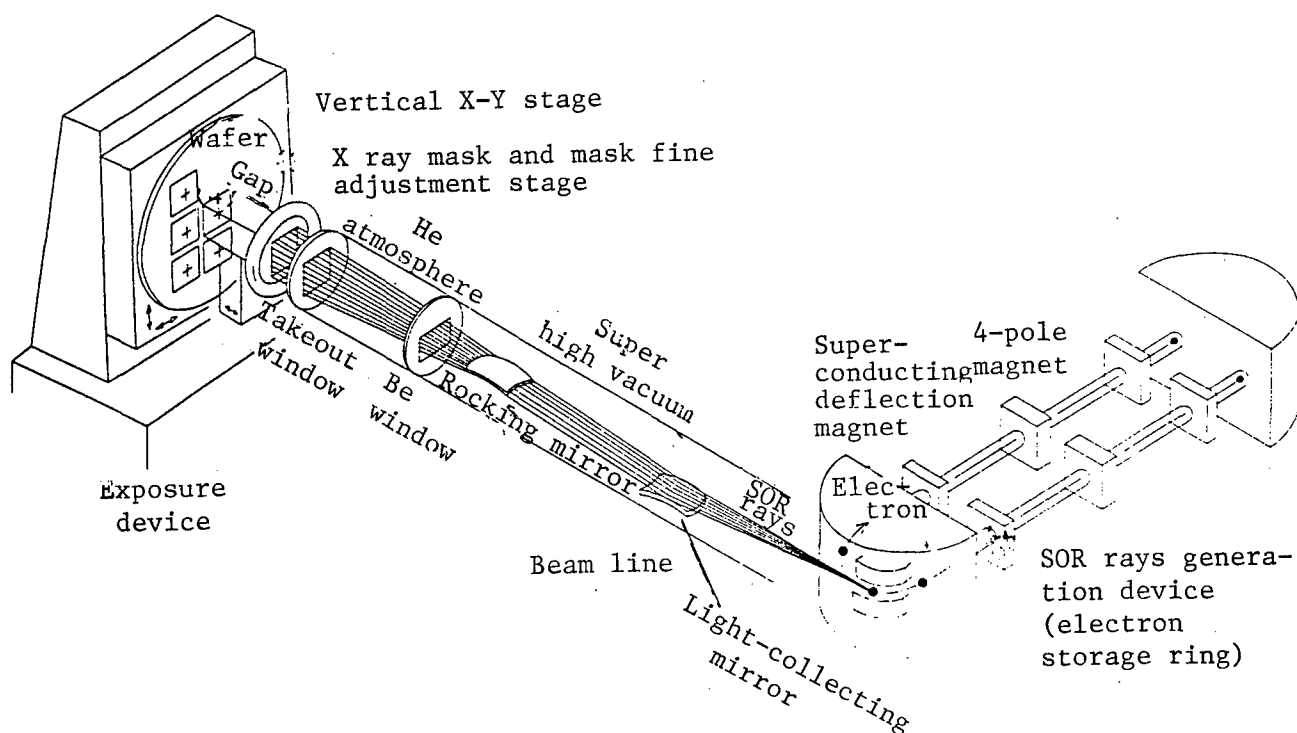
Taking Out SOR Rays and Transcribing LSI Patterns

To use the SOR rays generated by an accelerator ring or a storage ring for transcription of an LSI pattern, an X-ray mask that becomes the negative of a transcription pattern, an exposure device (aligner) which aligns the X-ray mask and a wafer at a precision of 0.1 μm or less, and a beam line that guides SOR rays from the ring to the aligner, are necessary. These techniques and devices are also indispensable as component elements of SOR lithography. Therefore, this laboratory is conducting R&D in parallel with R&D on the rings. Figure 5 shows the outline of SOR lithography that indicates such a relationship.

The aligner and beam line are configured so as to expose an X-ray mask and a wafer in the atmospheric environment. This is to keep to an allowable value or downward by the atmospheric heat dissipation effect the deterioration of positional precision of pattern caused by the thermal expansion which is the result of the X-ray mask temperature rise caused by the power of SOR rays. On the other hand, this method contains special features for the window material and structure to suppress attenuation of the SOR ray power at SOR ray takeoff window at the lower part of the beam line which guides SOR rays into the atmosphere.

The beam line has two mirrors. The first collects SOR rays which are radiated radially on a horizontal plane and increases the SOR ray power at the wafer position aimed at reducing exposure time. The second expands SOR rays in the longitudinal direction by rocking itself and makes large-area exposure possible. These mirrors remove ordinary X-ray components in the SOR rays. Furthermore, takeout windows of a ring remove the components whose wavelengths are longer than that of the soft X-rays. Removal of these unnecessary components from SOR rays causes the wafer to receive components of wavelengths 5 to 15 Å, components suitable for exposure.

In order to align a mask and a wafer at superhigh precision with the relative positional error of ±0.1 μm or less, the new technology is used for the detection method and the moving mechanism of the aligning marks set up on the mask and wafer.

47

Vertical X-Y stage

X ray mask and mask fine adjustment stage

Wafer

Gap

He atmosphere

Super high vacuum

Super-conducting deflection magnet

4-pole magnet

Takeout Window

Be window

Rocking mirror

SOR rays

Electron

Exposure device

Beam line

Light-collecting mirror

SOR rays generation device (electron storage ring)

Extremely fine patterns as fine as 0.2 μm are transcribed with the SOR rays emitted when electrons traveling at speed near the velocity of light are bent by a magnetic field.

Figure 5. Outline of Lithography

Aimed at Establishing Exposure Technique

This laboratory succeeded in taking out SOR rays with an ordinary conducting accelerator ring in June of last year, and with a superconducting small storage ring this year for the first time in the world. This method takes out SOR rays with the in-ring acceleration method which makes 15 MeV low-energy electrons incident on a superconducting small storage ring from a linear accelerator, accelerates the electrons to 600 MeV, and stores the electrons in the ring. This result was reported in newspapers on 9 February throughout this country.

The effectiveness of the SOR exposure technique has been confirmed with the newly developed beam line, X-ray mask, and aligner and by applying the SOR rays taken out from the ordinary conducting accelerator ring to the exposure in the wiring process of supermicro IC. Superhigh operation speed as high as 20 ps has been confirmed as a characteristic of trial manufactured MOSIC. Photograph 2 [not reproduced] is an example of transcribed patterns that realize 0.2 μm lines and spaces.

In the future, this laboratory intends to conduct research on improving SOR ray generator characteristics such as increase of SOR ray intensity by increasing the number of stored electrons and stabilization of electron

Synchrotron Orbital Radiation (SOR) Device

o Up-to-date technique for LSI pattern exposure

  Technique for processing LSI whose line width is 0.2 μm

  ┌───┐
  │ Technique to draw 2-mm-wide lines on Tokyo Dome │
  └───┘

o Small-sized and low-cost exposure device using superconducting magnet

o Paving the way to realization of ultra LSI (ULSI) → 64M-bit memory chip
  has become possible

Figure A
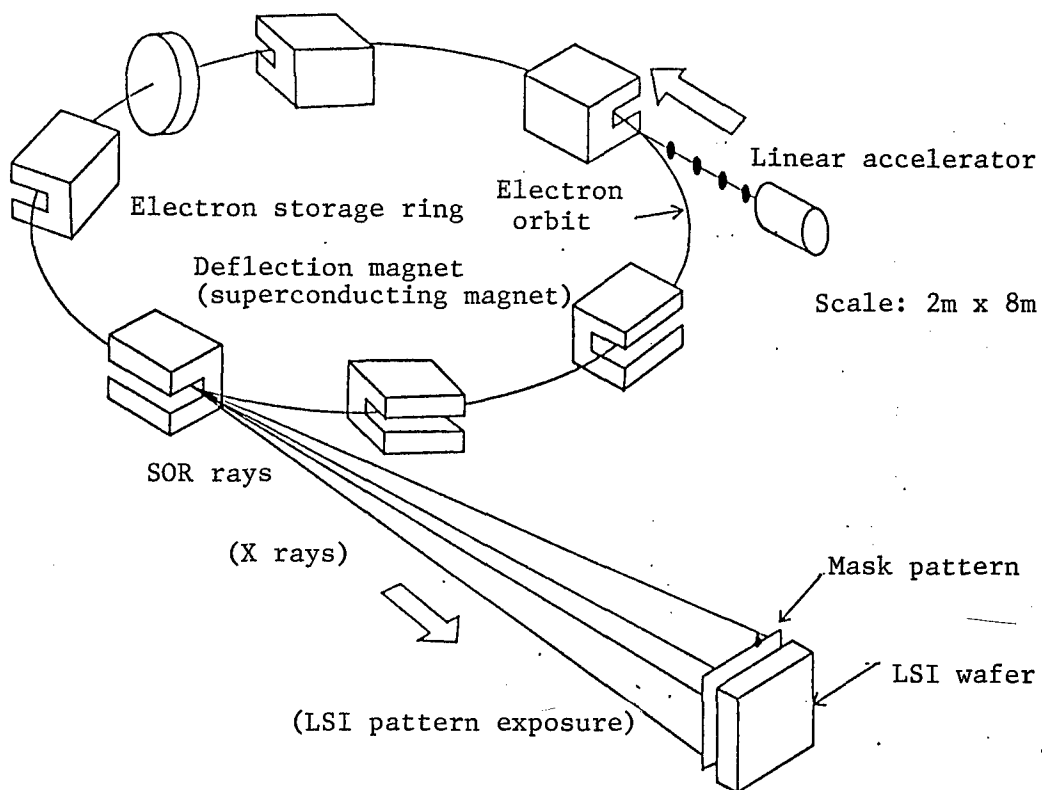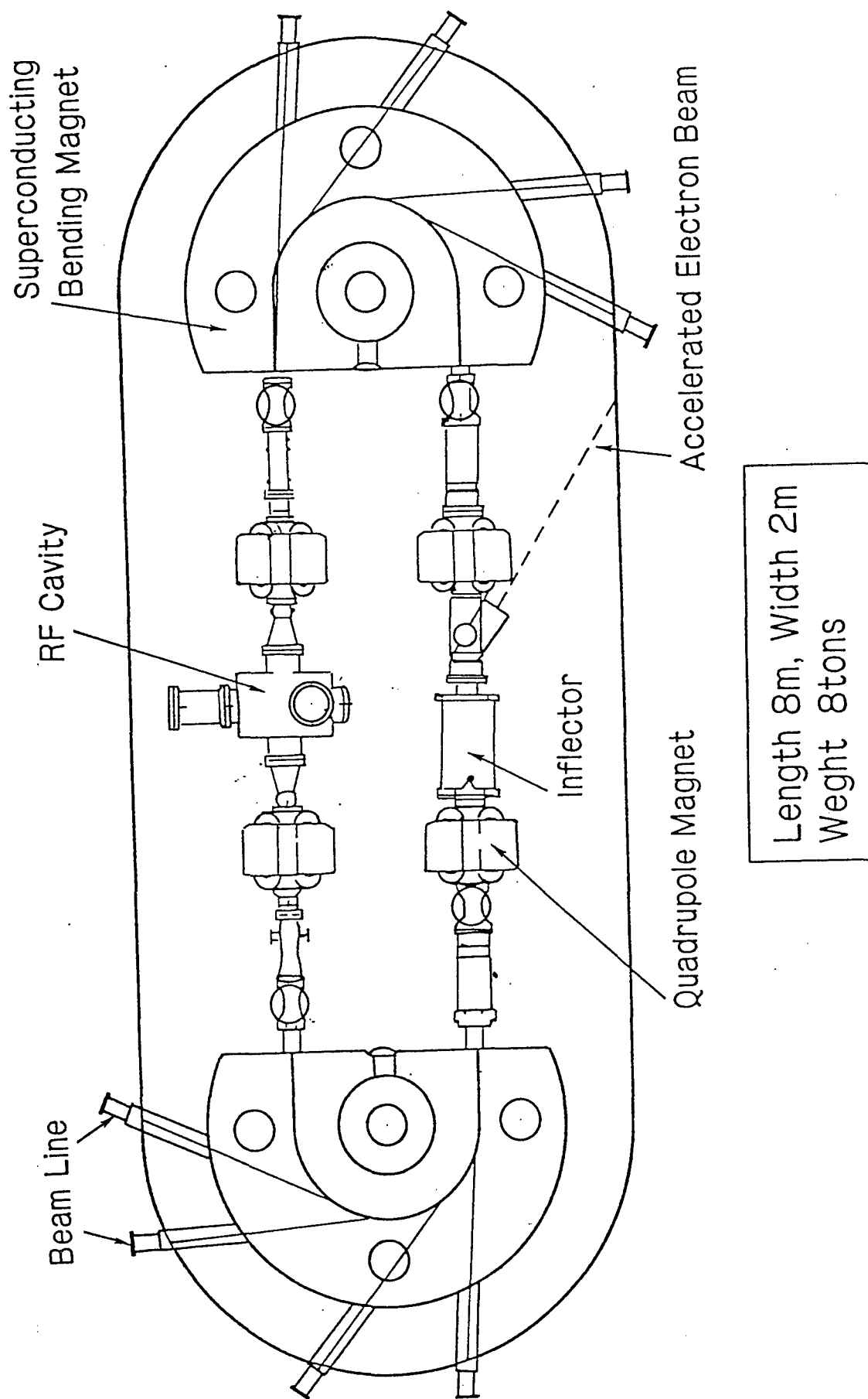
Figure B. Compact Storage Ring of SOR Equipment

Superconducting Bending Magnet

Accelerated Electron Beam

RF Cavity

Inflector

Quadrupole Magnet

Beam Line

Length 8m, Width 2m
Weght 8tons

orbit and on related techniques such as those related to the beam line, X-ray mask, and aligner, on the basis of the results of the R&D and experiments done so far, all aiming at realizing a more efficient and economical SOR lithography system.

References

X-Ray Lithography Technique, TSUKEN GEPPO, No 5 Vol 39, 1986.

- END -